Hydraulic studies for Liddell Power Station. Report No. 110, Vol. 4. Desanding works and high head line. December 1969.

Author:
Lai, K. K.; Yong, K. C.; Foster, D. N.

Publication details:
Commissioning Body: Electricity Commission of New South Wales
Report No. UNSW Water Research Laboratory Report No. 110, Vol 4.

Publication Date:
1969

DOI:
https://doi.org/10.4225/53/579ff2ebff04e

THE UNIVERSITY OF NEW SOUTH WALES
water research laboratory
Manly Vale, N.S.W., Australia

Report No. 110

https://doi.org/10.4225/53/579ff2ebff04e

HYDRAULIC STUDIES FOR LIDDELL POWER STATION

VOL. IV: DESANDING WORKS AND HIGH HEAD LINE

by

D.N.Foster K.K.Lai, and K.C.Yong

December, 1969

The University of New South Wales

WATER RESEARCH LABORATORY

HYDRAULIC STUDIES FOR LIDDELL POWER STATION

VOL. IV: DESANDING WORKS AND HIGH HEAD LINE.

by

D. N. Foster, K. K. Lai & K. C. Yong.

Report No. 110.

Final Report to the
Electricity Commission
of New South Wales 1969.

Key Words

Hydraulic Models
Liddell Power Station
Sediments
Settling Basins

0-85824-808-5

Preface.

The hydraulic investigations and model studies reported in this volume are part of comprehensive studies for the Liddell Power Station carried out by the Water Research Laboratory on behalf of the Electricity Commission of New South Wales.

The results are reported in a series of seven volumes of which this constitutes Volume IV.

Throughout the studies, the effective advice and co-ordination by the Electricity Commission staff is gratefully acknowledged and in particular those of Messrs. C.G.Coulter and N.Lamb.

The work was carried out by the staff of the Water Research Laboratory under the detailed supervision of Mr. P.B.Stone, Supervising Engineer, and the general direction of Mr. D.N.Foster, Senior Lecturer.

D.N.Foster
Senior Lecturer
Acting Officer-in-Charge.

Summary

Water for the initial filling and subsequent make-up of the cooling water lake at Liddell Power Station is obtained from the Hunter River by two stage pumping. River water, containing some sediment, is pumped by low head pumps to desanding chambers and settling ponds where the sediment is removed. After passing through the settling areas the clear water is lifted some 350 ft. by high head pumps to a break pressure tank located on nearby high ground. From the break pressure tank the water gravitates through a system of flumes and conduits to the cooling water reservoir some miles away.

Hydraulic investigations were undertaken to investigate some aspects of the operation of the proposed desanding works and hydraulic transitions in the gravity system between the break pressure tank and the cooling water reservoir. The results of these investigations are given in this report.

Index to Volumes.

Table of Contents

List of Figures.

List of Figures (cont'd.)

1. Settling Chamber

1.1 Introduction

Cooling water for the Liddell Power Station is pumped from the Hunter River by two stage pumping. The 1st stage river pumps handle sediment which must be settled out before entry to the 2nd stage high head pumps which transfer the water to the cooling pond. The settling chamber to handle the coarse sediment fraction (in excess of 100 microns) as initially proposed is shown in Figure 4 (after E.C. Hydraulic Research Note 50 Appendix H, Figure 1). The basin is approximately rectangular 100 ft. long x 20 ft. wide x 20 ft. deep. The inflow of 56 c.f.s. is by a 30 inch diameter inlet pipe which enters the basin through a 90° bend. Outflow from the basin is over a weir. A 3 ft. x 3 ft. gate is provided in the bottom of the basin to allow for sluicing of the settled sediment back into the river.

A model of the settling basin was built to study its settling and sluicing characteristics. Results of the investigation are presented in this section.

1.2 The Model

1.21 General

Details of the model are shown in Fig. 5. The linear scale of the model was 1:15 and other scales except sediment settling scale and scour time scale are determined from Froude model laws.

1.22 Sediment Size Scale for Settling

The appropriate scale for sediment size carried in suspension can be obtained from consideration of the settling properties of the sediment.

For a sphere of diameter d the fall velocity w is given by the relationship

$$w^2 = \frac{1.33}{C_d} \; gd \left(\frac{\rho_s}{\rho} - 1 \right) \qquad (1)$$

where C_d = coefficient of drag and is a function of the Reynolds Number

ρ_s = density of the solid

ρ = density of the fluid

The coefficient C_d as a function of Reynolds Number is given in Figure 6.

The settling velocities as computed from equation (1) for quartz sand (S.G. 2.65) at 70° F is shown in Figure 7.

For model similarity, the ratio of fall velocities should be the same as the velocity scale of the model, that is,

$$w_r = V_r = 1:3.87$$

For a given prototype sediment the required model material which will result in this velocity ratio can be determined from Figure 7. For a model scale of 1:15 the relationship between model and prototype is as shown in Figure 8.

1.23 Scour Time Scale

The Froudian time scale of 1:3.87 applies to flow paths and will not generally hold for sediment moved as bed load. At the present time there is no method by which this scale factor can be determined with any degree of certainty.

For river flow, and making certain simplifying assumptions as to bed form, an estimate of the scour time scale can be made using the various bed load formulae available (see Appendix A). Figure 9 shows time scales obtained in this way from the Kalinske and Einstein bed load formulae (Rouse 1949) as compared to the Froudian time scale of 1:3.87.

The present test conditions depart radically from river flow. Flow conditions are unsteady both during the draw down stage after the scour valve is opened and during the bed scour period when channel development is occurring over the floor of the basin. Consequently the analysis above can be expected to give no more than an indication of the variability in the time scale that might be expected. For these reasons model results on scour within the basin have been given in model times. Figure 9 can be used with judgement to obtain approximate prototype equivalents.

1.3 Theoretical Considerations

Most of the work published to date has developed around the theory of an ideal settling basin as first developed by Hazen (1904). Arbitrary modifications are made to allow for variation in the theory for the practical case.

In the ideal tank it is assumed that all particles settle freely at their terminal velocities; flow through the basin is uniform and steady; the distribution of sediment inflow is constant over the cross section; turbulence, eddy currents, density currents and thermal disturbances are absent; and particles once settled will not be re-entrained.

Under these conditions it can be easily shown that, for a rectangular tank, the terminal velocity (w_{min}) of the smallest particle which will be completely settled out is

$$w_{min} = \frac{Q}{LW} = \frac{Q}{A_s} \qquad (2)$$

where Q = inflow
L = basin length
W = basin width
A_s = surface area

For particles with fall velocities less than w_{min} the removal ratio is given by

$$\frac{q_i - q_o}{q_i} = \frac{WL}{Q} w \qquad (3)$$

where q_i = inflow of sediment/unit width
q_o = outflow of sediment/unit width
w = terminal velocity of sediment

The term Q/WL is generally referred to as the "overflow rate". It is of interest to note that equations (2) and (3) are independent of depth and therefore of detention time.

The variation in practice from the behaviour of an ideal basin has been discussed at length in the literature with considerable controversy. A review of published work is presented by Miller (1964). As yet the literature gives no clear idea of the best form of design and the majority of effort has attempted to obtain ideal flow conditions by extensive and sometimes excessive use of baffles.

Babbitt et al (1962) suggest the use of perforated baffles with velocities through the diffuser-wall slots or perforations of between 0.4 and 0.8 f.p.s. with corresponding head loss of 0.01 to 0.02 ft.

The effect of turbulence, hindered settling, eddy currents etc. is to

retard the rate of clearing and so increase the required surface area over that indicated by ideal basin analysis.

There are a considerable number of published formulae for hindered settlement as summarised by Miller (1964). These equations could be used in place of the fall velocity of discrete particles for analysis of the ideal settling basin. However, with the present state of knowledge, such analysis could be expected to serve only as a guide to possible behaviour in practice. Richardson et al (1961) from experiments on uniform systems of particles of various shapes proposed the formula:

$$w_c = w(1-c)^x \qquad (4)$$

where w_c = settling velocity of the suspension
w = settling velocity of a discrete particle
c = volumetric particle concentration
x = a function of the particle Reynolds number $(\frac{wd}{\nu})$
(For spherical particles and Reynolds number less than 0.2, $x = 4.8$)

Where sediment remains undisturbed after reaching the bottom the primary effect of turbulence is to delay the settling time. For steady state conditions Dobbins (1944) found from diffusion considerations that:

$$V\frac{\partial c}{\partial x} = \varepsilon y\frac{\partial^2 c}{\partial y^2} + \left(w + \frac{\partial \varepsilon y}{\partial y}\right)\frac{\partial c}{\partial y} + \varepsilon x\frac{\partial^2 c}{\partial y^2} \qquad (5)$$

V = mean fluid velocity x, y
c = local concentration of sediment
$\varepsilon x, \varepsilon y$ = mixing coefficients in x and y directions
w = fall velocity of sediment
x = co-ordinate along the length of the basin
y = co-ordinate vertically above the bed

No general solution of equation (5) has been found. To obtain an approximate solution for application to the settlement of discrete particles in a settling tank Camp (1946) has made a number of simplifying assumptions

(i) $\varepsilon x\frac{\partial^2 c}{\partial x^2}$ is zero

(ii) velocity is constant throughout the depth

(iii) εy is constant and given by:

$$\varepsilon y = 0.075\, H\sqrt{\frac{\tau o}{\rho}}$$

where H = basin depth

τ_o = bed shear = $\frac{\gamma f V^2}{8g}$

f = Darcy friction factor

V = mean velocity

It should be noted that assumptions (ii) and (iii) are incompatible since the third assumption corresponds to a parabolic velocity distribution.

On these premises Camp has obtained a graphical solution to equation (6) as shown in Figure 10 which can be used as a guide to the design of basins settling discrete particles.

From the simple theory of sedimentation it is apparent that the most economical tank is that which has the least possible depth which will prevent scour and re-entrainment of the settled sediment. If turbulence is considered, the amount settled is dependent somewhat on depth as indicated by Figure 10. This effect is small and a 50 pc. decrease in depth will on average reduce trap efficiency of sediment by not more than 5 pc. For economy, therefore, the conclusion still holds that the depth should be made as small as is consistent with no scour.

Flocculation, eddy and density currents, thermal disturbances and hindered settlement present added difficulties and successful design of settling chambers is still largely a matter of experience. Hydraulic models can be used as an aid to the design but owing to the difficulty of establishing exact scale relationships, interpretation of the model results is difficult.

1.4 Application of Theory to Proposed Settling Basin

For a basin 100 ft. long x 20 ft. wide and an inflow of 56 c.f.s. equation (2) indicates a minimum fall velocity of 0.028 f.p.s., for a particle which will be completely settled out in an ideal basin. For discrete particles, the diameter of a sand grain having such a fall velocity is approximately 100 microns (see Figure 7). Departure in practice from the ideal basin will reduce trap efficiency.

For a sediment concentration of 5000 ppm the settling rate of the suspension (from equation 4) is 98 pc of that for a discrete particle. The effect of concentrations up to this order of magnitude on the behaviour of settling basins is therefore small.

Allowing for the effects of turbulence in reducing the settling rate of a discrete particle, the efficiency of the proposed basin in settling out particles of various sizes can be estimated from Figure 10. Assuming an arbitrary value of f equal to 0.024 and settling velocities as given in Figure 7 the trap efficiency of the proposed basin for a range of particle sizes has been computed and plotted in Figure 11. This indicates a trap efficiency of 92 pc. for 100 micron particles as compared to 100 pc. obtained from ideal basin analysis. For 100 pc. settlement of 100 micron material the basin length would need to be increased to 150 ft.

Based on the recommendations of Babbitt et al (1962) the hole area in a perforated baffle to produce uniform flow in the basin, should be between 80 and 160 sq. ft.

1.5 Test Results

1.51 General

Unless otherwise stated, all figures given in this report are in prototype equivalent as based on the scale relationship developed in Section 1.2.

1.52 Detention Times

For an ideal basin of the proposed dimensions and without any displacement by settled sediment, the detention time (T) is theoretically 715 seconds. In practice some of the fluid passes through the tank in less time than the theoretical detention period whilst some takes longer. This results in a distribution of detention times dependent upon the paths of the water particles. Variations from the ideal basin are accentuated by eddy currents, high inlet velocities, dead spaces within the tank and accumulation of settled sediment.

Detention times for the proposed basin were determined by injecting neutrally buoyant particles into the inflow and timing the passage of the particles through the basin. Tests were run for the following conditions:-

(i) Tank with no settled sediment and without baffle

(ii) Tank with no settled sediment but with perforated inlet baffle

(iii) Tank half filled with sediment without inlet baffle

(iv) Tank half filled with sediment with perforated inlet baffle.

The baffle used in the tests was a perforated board with 81 holes

1'3" diameter evenly spaced over the cross-sectional area. The total hole area was 100 sq. ft. and the baffle was located 6 ft. downstream of the inlet end of the settling chamber.

To undertake the tests with the tank half filled by sediment, 5.9 cu.ft. of Sydney sand (median diameter 0.21 mm) was introduced into the model settling chamber over an interval of approximately 3 hours. In the full scale installation this corresponds to the introduction of 20,000 cu.ft. of sand of 0.65 mm median diameter over a period of approximately 11.5 hours. Size grading of the Sydney sand as used in the tests is shown on Figures 12 and 13 and the settlement pattern in Figure 15 at time zero. After settlement, the surface of the sand was stabilized by coating the surface with cement mortar before carrying out the tests.

The size grading of silts, sands and gravels which will enter the river pumps for various river flows is not known. Samples of the river bed in the vicinity of the pump have been taken and size graded (J.R.Ewers and D.M.Stone, 1965). These show the presence of material of between 0.04 mm and 6 inch diameters. The design of the river pump has been aimed at excluding as much of the bed load as possible and therefore it is to be expected that the majority of the sand which enters the pumps will be from the lower end of these gradings. However, the possibility that some coarse material will at times enter the settling chamber must be kept in mind especially when investigating the scouring capabilities of the basin.

The median diameter of sand taken from the river bed at the pump location is approximately 0.3 mm which is approximately that used during the tests. Suspended sediment samples taken during a "fresh" in the river in December, 1965 (max. discharge 1300 c.f.s.) have indicated material in suspension of between 5 and 500 microns at concentrations up to about 2000p.p.m. Suspended sediment samples taken at Singleton by the Hunter Valley Research Foundation show concentrations of 1120 p.p.m. at discharges of 1300 c.f.s. but no information is available on the size of material in suspension. For higher flood flows it can be expected that the size and concentration of suspended sediment will increase. The settlement pattern within the basin will depend upon the relative concentrations of the various sediment sizes entering the settling chamber. With the limited data available, it is impossible to predict what this may be, and for this reason, it is difficult to know to what extent the settlement pattern obtained in the model with Sydney sand (Figure 15 at time zero) is representative of the full scale basin. On the existing evidence it is felt that it represents a severe but not unlikely condition but the results of the

operation of the basin in the half full condition should be assessed with the above comments in mind.

The distribution of detention times for each of the test conditions has been plotted non-dimensionally in Figure 14. In plotting these graphs, the theoretical detention times for the tank empty and tank half-filled by sediment have been taken as 715 and 358 seconds respectively.

In Section 1.3 it was shown that detention time is not a measure of the efficiency of the basin. A reduction of 50 pc. in the depth of the basin which will halve the detention period will have little effect on the trap efficiency of the basin. The distribution of detention times is, however, a measure of hydraulic effects such as short circuiting and dead spaces and for maximum efficiency the distribution should be as narrow as possible.

The benefit of a baffle in improving the flow distribution through the settling chamber (no sediment deposition) is obvious from a comparison of Figures 14a to 14b. Without a baffle two vertical rollers were formed on each side of the inlet pipe and these persisted for about half the basin length before they were dissipated. The baffle was very effective in eliminating the inlet effects and further improvement could be expected if the hole area were reduced.

The benefit of the baffle was reduced as sediment entered the settling chamber. The sand used in the tests settled out initially in the vicinity of the inlet pipe and the baffle soon became buried and therefore became ineffective as can be clearly seen from a comparison of Figures 14c to 14d. With the test sand of median diameter 0.42 mm (size grading as shown in Figures 12 and 13) the baffle was virtually ineffective after the introduction of 7000 cu. ft. of sand (20 pc. basin capacity). This latter figure should be used only as a guide in estimating the efficiency of the baffle, as sediment of smaller diameter will require a much larger volume before the effect of the baffle is completely eliminated. The incorporation of a baffle in the design should be considered in the light of the above comments.

Where dead spaces exist in a settling chamber, the effective volume of the tank is less than the total volume and the relative time to the centre of gravity of the distribution curve will be less than the theoretical detention time for an ideal basin. In all the distribution patterns (Figure 14) dead spaces are evident but they are particularly noticeable when the tank is half filled with sediment as would be expected from the way in which the

sand settles. Where the dead space is at the bottom of the chamber a larger reduction in the efficiency does not necessarily result. Because of the dead space the effective depth of the basin is reduced, but, as discussed in Section 1.3 depth has only a secondary effect on basin efficiency. If dead spaces are to be eliminated the use of multiple baffles along the length of the basin may be desirable.

1.53 Trap Efficiency

A measure of trap efficiency of the basin was obtained by feeding sediments of various sizes into the model. The settled material was weighed and compared with the weight of sediment introduced. Four materials were tested in the model with size gradings as shown in Figure 13. The equivalent prototype gradings for sands of S.G. = 2.65 as based on the scale relationships given in Section 1.2 are shown on Figure 13.

The results of the tests are tabulated in Table 1.1.

Using a step form of the sediment size gradings (Figure 13) the theoretical trap efficiency can be calculated as per Camp (1946) from Figure 10. The computed trap efficiencies for sand 2 and sand 1 and sand 0 are 99, 98 and 35 per cent respectively which agree closely with that recorded in the model when a baffle was incorporated in the design (c.f. 98.5; 99 and 34.5 per cent). This result suggests that the model scaling laws for sediment sizing are satisfactory.

The trap efficiency of the basin is increased slightly by the use of a perforated inlet baffle. The effectiveness of the baffle is reduced, however, as the basin fills with coarse material and submerges the baffle.

As deposition occurs within the basin there is some loss of efficiency. This reduction is small in comparison to the reduction in storage area which confirms the comments made in Section 1.3 that the depth of the basin has only a secondary effect on basin efficiency.

1.54 Scour Tests

To observe how the settling chamber would scour during the flushing period, the model was half filled with Sydney sand (0.65 mm median dia.) in the manner described in Section 1.52 and then the scour valve opened and the discharge of 55 c.f.s. introduced through the inlet bend. The bed profiles at different times were observed and photographed. Three

Table 1.1: Trap Efficiency of Proposed Basin

Description of Test	Model Material	Median dia. of Material (mm)	Equiv. median dia. of prototype sand of SG2.65 (mm)	Average Inflow Sediment conc. (ppm)	Wt. of material introduced (oz)	Wt. of material retained (oz)	Trap Efficiency (pc)
(1)	(2)	(3)	(4)	(5)	(6)	(7)	(8)
1. Tank empty - no baffle	Sand 3	0.225	0.65	336	389	389	100
	do.	0.225	0.65	340	327	327	100
	Sand 2	0.098	0.23	322	310	304	98
	do.	0.098	0.23	275	319	310	97
	Sand 1	0.086	0.21	178	240	222	92.5
	Fly Ash	0.034	0.055	182	211	60	28.5
2. Tank empty- with baffle	Sand 2	0.098	0.23	213	288	284	98.5
	Sand 1	0.086	0.21	154	208	206	99
	Fly Ash	0.034	0.055	218	252	73	34.5
	do.	0.034	0.055	295	68	20	29.5
3. Tank $\frac{1}{2}$ Full - no baffle	Sand 3	0.225	0.65	184	320	318	99.5
	do.	0.225	0.65	184	320	320	100
	Sand 2	0.098	0.23	165	320	304	95
	Fly Ash	0.034	0.055	137	52.5	10.5	20
	do.	0.034	0.055	210	97	16	16.5
4. Tank $\frac{1}{2}$ full - with baffle	Sand 3	0.225	0.65	166	320	314	98
	Sand 2	0.098	0.23	284	284	252	89
	Sand 1	0.086	0.21	249	320	275	86

tests were run without an inlet baffle and three with. For four of the tests (two for each condition) the sand tended to hang up on one of the side walls of the tank as shown in Figures 1 and 2. In the other two tests the scour developed evenly across the bed and bed profiles at various times have been plotted in Figure 15.

The effect of the sand hanging up against the side walls is to increase the time necessary to scour out the chamber. Figure 15 therefore represents the best condition likely to be attained in the prototype.

In the discussion of the results, volumes of sand are given in prototype equivalents but because of the inexact value for scouring time scale (see section 1.23) times are given to model scale. Prototype times corresponding to these values can be approximately obtained from Figure 9.

From Figure 15 the approximate volume of sand remaining in the tank at various stages of flushing have been computed and are shown plotted in Figure 16. From this graph it would appear that the inlet baffle has no appreciable influence on scour behaviour.

During flushing five stages were noticed, the bounds of which are indicated approximately in Figure 16.

(i) For about 20 seconds after opening the scour valve the sand was redistributed within the basin and no outflow of sand occurred.

(ii) After the initial redistribution of sand, rapid scouring of the bed occurred. The initial large bed slopes induced high velocities but as scour developed the bed slopes, and consequently the scour rates, were reduced. After about 1 m. 40s. further reduction in the bed slope was prevented by the concrete floor of the settling chamber.

(iii) Between 1m. 40s. and 3m. 20s. after opening of the scour valve flow velocities were controlled by friction of the sand bed and the slope of the concrete floor of the stilling basin.

(iv) After 3m. 20s. the floor of the basin near the inlet had been swept clean of sediment. Bed velocities were increased because of reduced friction and significant turbulence was induced at the junction between the sand bed and the concrete floor of the settling chamber. This resulted in a local increase in the scour rate which continued for about 50 seconds.

(v) 4m.10s. after opening the scour valve, flow at the downstream end of the basin was controlled by the discharge characteristics of the gate. Velocities were very much reduced and scour rates were very small. Because of this control some sediment was never swept out of the basin.

The bounds of the different stages and the times described above should be considered only as qualitative since they take no account of variations in sediment sizes and cohesion, inflow concentrations and tendency of the sediment to hang up against the wall of the chamber. However, they do serve to indicate modifications which could be made to improve the performance of the basin.

Changes to the basin geometry will have no effect on stages (i) and (ii). Scour rates during stages (iii) and (iv) could be increased by increasing the bed slope of the floor of the settling chamber. The increased scour rate resulting from an increased slope can be estimated from one of the bed load formulae. Using Einstein's bed load function the ratio between the rate of sediment transport (q_{s1}) on slope S_1 to the rate of sediment transport (q_{s2}) on slope S_2 for a given material is

$$\frac{q_{s1}}{q_{s2}} = \frac{y_1^3 S_1^3}{y_2^3 S_2^3} \qquad (6)$$

For a given discharge, Manning's equation and the equation of continuity give

$$\left(\frac{y_1}{y_2}\right) = \left(\frac{S_2}{S_1}\right)^{3/10} \qquad (7)$$

Substituting this value for $\frac{y_1}{y_2}$ in equation (6) gives

$$\frac{q_{s1}}{q_{s2}} = \left(\frac{S_1}{S_2}\right)^{21/10} \qquad (8)$$

Note: An alternative approach based on Shields' equation for Sediment transport (Rouse 1949 p. 816) gives $q_s \propto S^{7/5}$)

Thus doubling the slope increases the rate of sediment transport approximately three to four fold.

The slow scour rate observed during stage (v) was the result of

insufficient hydraulic capacity of the scour valve. This could be rectified by either increasing the size of the opening and/or locally lowering the opening below the floor level of the basin to provide a critical depth control at the downstream end of the chamber.

1.6 Conclusions

(i) The model results show acceptable agreement with the theoretical work by Camp (1946) and can therefore be expected to indicate prototype trends satisfactorily. However, as model scaling laws are based on equations describing phenomena which are at the moment improperly understood, the model results should be considered as semi-quantitative only.

(ii) The estimated trap efficiency (basin empty) is 92 per cent for material of 100 micron diameter. For 100 per cent settlement of this material the surface area of the basin would need to be increased by 50 per cent.

(iii) Settlement of sediment within the basin reduces the trap efficiency slightly. This reduction is small, however, compared to the reduction in storage area and indicates that depth of the basin has only a secondary effect on basin efficiency.

(iv) Distribution of flow through the basin is very uneven unless an inlet baffle is provided.

(v) Trap efficiency of the basin is increased by using an inlet baffle. However, the effect of the baffle is reduced as sediment is deposited and the baffle is buried. The use of multiple baffles may be more advantageous for this reason.

(vi) Flushing tests have been undertaken for one material size only (650 microns). Results of tests on this material indicate that under the best operating conditions 50 per cent of the material will be removed in 70 seconds (model) (basin initially half full) and 75 per cent of the material in 3 minutes 20 seconds (model). Removal of the last 10% is very slow because of the control to the flow imposed by the size of the scour hole.

(vii) Flushing time for the basin could be reduced by:-

(i) enlarging the outlet and/or by locally lowering of the opening below the floor level of the basin to provide a critical depth control at the downstream end.

(ii) steepening of the bed slope of the chamber consistent with required storage capacity and geological conditions.

(viii) The scour tests indicated a tendency for sand to hold up against the sides and consequently to increase the time for flushing.

(ix) The scour rate was not affected by an inlet baffle.

2. Wasteway for Settling Chamber

2.1 Introduction

During flushing of the settling chambers, sediment is sluiced into a wasteway which tranports it back to the river. Adjacent to the settling chambers the wasteway is rectangular in shape with side entries to the settling chambers. Downstream there is a transition from the rectangular section to a circular conduit. Both conduits are laid on a 1:20 grade.

A model of the wasteway was constructed to study its operation and in particular the likelihood of blockage under extreme conditions. The results of this investigation are discussed below.

2.2 The Model

The full length of the wasteway was modelled together with the settling chamber most remote from the outlet. This was considered to be the worst possible condition for operation. The scale of the model was 1:15 as had been previously used for the settling chamber. Other scales are as described in Section 1.2. The general layout of the model is shown in Figure 17.

2.3 Test Procedure

The settling chamber was initially half filled with sediment to approximate conditions after a long period of operation. The scour gate from the settling chamber was then opened and the behaviour of the wasteway observed. Tests were carried out using both Sydney sand and fly ash in the model.

The above tests were repeated with the settling chamber three quarters filled with sediment to study the possibility of blockage under extreme but most unlikely conditions.

2.4 Discussion of Results

The tests showed that the design of the wasteway was satisfactory. There was no tendency for blockage to occur and after the settling chambers had been cleared of sediment the wasteway was scoured clear.

3. Pipe Inlet Transition

3.1 Introduction

Cooling water to the Liddell Power Station is obtained by pumping from the Hunter River. Water from the river is pumped to a break pressure tank located on nearby high ground. From the break pressure tank the water is gravitated to the cooling water reservoir through a system of unlined open channels and high velocity flumes. A typical section along the system is shown in Figure 18.

To ensure that flow in the open channels enters the high velocity flumes smoothly and efficiently, an inlet transition between the two is to be provided. In this section the design of such a transition is discussed and its operation tested by hydraulic model. The design was aimed at keeping the transition length as short as possible whilst maintaining trouble free operation.

3.2 General Design Considerations

The high velocity flume which joins the two open channels shown in Figure 18 has a slope of approximately 0.10. Flow in the flume is super-critical and details of the design of pipe diameter are given in Appendix B.

From considerations of cavitation, air entrainment and flow stability a 3.75 ft. diameter pipe has been chosen. At the design discharge of 200 c.f.s. the flow depth (air-water mixture) is expected to be 0.75 D for a Manning roughness coefficient of 0.02.

At the transition from the earth channel to the high velocity flume a drawdown profile will result with critical depth occurring at the break of grade where the flow enters the pipe. Critical depth can be computed from the relationship

$$\frac{Q^2 T}{g A_c^3} = 1 \qquad (9)$$

where Q = discharge in c.f.s.
T = width of flow surface at critical depth in ft.
A_c = cross sectional area of flow at critical depth in ft.^{2}
g = gravitational constant = 32.2 ft/sec^2.

Critical depth computed from equation (9) with the aid of Figure 20, is 3.68 ft. as compared to the actual pipe diameter of 3.75 ft. As critical depth is so close to the actual pipe diameter it is probable that any local disturbance which affects the location of critical depth would result in submergence of the pipe entrance leading to flow instability and surging. To avoid this it was proposed to use a transition section in the initial region of flow acceleration. The design of such a transition and the results of model tests undertaken on the transition are discussed in the following section. These serve as an example on which the design of other transitions in similar situations may be based.

If an inlet diameter of 5.2 ft., (approximately 1.5 times the pipe diameter) is used, then critical depth is found to be 3.98 ft. or 0.77 times the inlet diameter. The critical velocity is 11.4 f.p.s. The length of the drawdown curve between the location of critical depth and normal flow in the pipe can be approximated from energy considerations with friction neglected. Referring to Figure 21, the Bernoulli equation can be written as

$$d_c + \frac{V_c^2}{2g} + S.L. = d_n + \frac{V_n^2}{2g} \qquad (10)$$

where d_c = critical depth at the break of grade in ft.
v_c = critical velocity at the break of grade in ft/sec.
d_n = normal depth of flow in the pipe in ft.
v_n = velocity of flow in the pipe in ft/sec.
S = slope of the pipeline
L = transition length in ft.

Solving for L using the same slope as the pipe gives

$$L = \frac{\left(d_n + \frac{V_n^2}{2g} - d_c - \frac{v_c^2}{2g}\right)}{S}$$

$$= 10 \times \left\{2.55 + \frac{(25.2)^2}{2g} - 3.98 - \frac{(11\ 4)^2}{2g}\right\}$$

$$= 64.2 \text{ ft.}$$

The drop between the inlet and the section where the flow attains its normal depth will be

Drop = S.L. = 6.42 ft.

The function of the inlet transition is to provide a length for the flow acceleration to take place. It is feasible to have a very steep slope at the inlet so that the acceleration can take place within a much shorter distance and hence a much shorter transition can be used. Keeping the diameter of the pipe at the inlet at 5.2 ft. and the drop between the inlet and the section where the flow attains its normal depth at 6.42 ft. a form of the inlet transition as shown in Fig. 22 is suggested. Assuming the bed of the approach channel to be horizontal, the inlet has a 1 to 1 slope for a length of 8.5 ft. After this length, the invert of the pipeline is at the slope of 1 in 10 as dictated by topography. The 5.2 ft. diameter at the inlet is reduced to 4 ft. 2 in. at the break between the 1 in 1 grade and the 1 in 10 grade. The diameter of the pipe along the 1 in 10 grade is further gradually reduced to the pipe diameter of 3.75 ft. over a distance of 5 ft. The total drop between the inlet and the end of the transition is 6.5 ft. which is approximately the required value of 6.42 ft. from the foregoing computations.

The model study of the pipe inlet transition described in the following sections is based on this design.

3.3 Model Design

A linear scale of the model was 1:25. Other scale ratios as determined from the Froude model relationships are as follows:-

Discharge scale	1:3100
Velocity scale	1:5
Roughness scale	1:1.71

The design of the prototype flume is based on a Manning's n of 0.02. Consequently the required model roughness is 0.012 which is closely approximated by "perspex" which was used to construct the model.

The total length of the pipeline in the prototype is about 1200 ft. In the model only 300 ft. of the prototype length was modelled as this was sufficient for uniform flow to develop. The cross section of the delivery channel was trapezoidal with a base width of 6 ft. and $1\frac{1}{2}$ to 1 side slopes. Over the last 20 ft. of the approach channel the width of the channel was narrowed down to the inlet diameter of the pipe by using two straight vertical walls. On the downstream end of the model a pipe bed in the form a ski-jump was provided. This was one suggestion for energy dissipation at the discharge end of the high velocity flume and

was incorporated in the model to study flow behaviour in its vicinity. The pipe was provided with air vents to enable air taken into suspension to be replaced should this prove necessary during the model tests. A general layout of the model is shown in Figure 23.

3.4 Test Details

Tests were undertaken at the design discharge of 200 c.f.s. and also at higher flow rates to investigate the possibility of reducing the freeboard and pipe diameter required. Three conditions of air venting were studied as follows:-

(i) No air vents
(ii) Air vent immediately after the inlet transition
(iii) Air vents at 150 ft. intervals along pipeline

3.5 Test Results

At the design discharge of 200 c.f.s. flow through the transition and pipeline was even and steady. Flow conditions were not affected by venting as sufficient air could be drawn through the inlet to satisfy the air demand. Operation of the transition was satisfactory.

At discharges higher than the design conditions the flow in the pipeline exhibited different characteristics for different conditions of venting. Test results are shown in Figure 24.

With no air vents, air was drawn into the pipe through the pipe inlet. As flow was increased above the design discharge the air demand was raised whilst the air intake area was reduced. At a discharge of 240 c.f.s. the noise level increased appreciably and fluctuations of the water surface became noticeable. The air inflow through the entrance depressed the water surface and it was possible to increase the discharge to 310 c.f.s. whilst still maintaining channel flow in the pipeline. At 310 c.f.s. pipe full flow occurred,the discharge then being a function of head difference along the pipe line. Under these conditions water levels in the approach channel increase rapidly with increasing flow (Figure 24).

With the pipeline vented immediately after the inlet transition air demand in the pipe could be satisfied through the vent. At a discharge of 240 c.f.s. the inlet transition flowed full whilst the pipeline flowed part full. The noise noticed with unvented conditions was not present. The flow at the inlet can be termed "sluice flow", the discharge being dependent on the ratio of depth of water in approach channel to the throat

diameter at the end of the transition. Under these conditions water levels in the approach channel increase rapidly with increasing discharge (Figure 24).

Flow profiles for both vented and unvented conditions at various flow rates are shown in Figures 25 and 26.

3.6 Theoretical Considerations

The test results show that flow in the transition and pipeline may lie in either of two flow regimes. Below a critical discharge flow occurs as free surface flow with a critical depth control at the inlet. Under these conditions water depths in the inlet channel increases fairly slowly with discharge. Above the critical discharge the control shifts from a critical depth control to either pipe flow for an unvented pipeline or "sluice flow" through the transition for a vented pipeline. Under these conditions flow depth in the approach channel increases much more rapidly with discharge (Figure 24).

To avoid deep and expensive channels and the possibility of surging, it is apparent that flow conditions through the transition and channel should always be maintained as free surface flow. With the present design and a maximum flow rate of 200 c.f.s. it is apparent, from Figure 24, that this is achieved with a sufficient margin of safety.

For the design of similar structures it is of interest to attempt to predict theoretically the break away point for the two flow regimes and to compare the predicted results with that obtained from the model. For flow with critical depth control the depth-discharge relationships can be computed from the critical depth relationships. For pipe flow or "sluice flow" the depth-discharge relationship may be estimated from energy considerations. Details of the theoretical computations are given in Appendix C and a comparison between experimental observations and theoretical predictions are shown in Figure 27. The agreement is quite good, especially when friction is taken into account.

The procedures developed in Appendix C can therefore be used for the design of similar transitions to that tested where the design conditions are changed.

3.7 Conclusions

Design methods have been developed for a short transition structure

between an open channel on a mild slope and a steep high velocity conduit for which the acceleration region is kept as short as possible. These methods have been applied to a typical section along the Liddell cooling water supply system. Model tests have shown the methods to be satisfactory and of general application to similar structures where the design requirements for slope, discharge etc. are changed. In each case however, attention should be given to each of the following factors:-

(i) Flow regime and geometry necessary to maintain free surface flow.

(ii) Flow stability
(iii) Cavitation
(iv) Air demand.

Appendix A: Approximate Time Duration Scales for Sediment Transport on a Plane Bed.

Using Brown's form of the Einstein bed load function (Rouse 1949) the volume rate of transport for unit width of sediment of constant specific gravity can be expressed as

$$q_s \propto \frac{F\, y^3 S^3}{d^{3/2}} \qquad \text{A1}$$

where q_s = volume rate of sediment transport for unit width
F = dimensionless function of the fall velocity
S = energy slope
y = depth flow
d = grain diameter of the sediment

The discharge per unit width can be approximated by the Manning equation

$$q = \frac{1.49}{n}\, y^{5/3}\, S^{\frac{1}{2}} \qquad \text{A2}$$

where q = discharge per unit width
n = Manning roughness parameter

A number of investigators as reported by Foster (1966) have shown that for a plane bed n is related to sediment size by the expression

$$n = \frac{d}{k}^{1/6}$$

where k = a constant

Substituting into equation A2 and simplifying yields

$$y \propto \frac{q^{3/5}\, d^{1/10}}{S^{3/10}} \qquad \text{A3}$$

which on substitution into equation A1 gives

$$q_s \propto \frac{F q^{9/5}\, S^{21/10}}{d^{12/10}} \qquad \text{A4}$$

If slopes are taken to be the same in the model and the prototype the scour time scale from equation A4 is

$$t_{sr} = \frac{L_r^2\, d_r^{1.2}}{q_r^{1.8}\, F_r} = \frac{d_r^{1.2}}{L_r^{0.7} F_r} \qquad \text{A5}$$

If the same procedure as above is used with the Kalinske bed load function as approximated by Brown (Rouse 1949) the scour time scale is given by the expression

$$t_{sr} = \frac{d_r^{0.75}}{L_r^{0.25}} \qquad \text{A6}$$

Figure 9 shows a plot of equations A5 and A6 for the sand size scale ratios based on settling (Figure 8). The difference results from the form of bed load function used to define sediment movement.

Appendix B: General Considerations in the Design of the Pipe.

When a pipe is running part-full with a free surface, the velocity of the flow, and hence the discharge, can be computed from the Manning formula as -

$$V = \frac{1.49}{n} R^{2/3} S^{1/2} \qquad B1$$

$$Q = \frac{1.49}{n} AR^{2/3} S^{1/2} \qquad B2$$

where
- V = velocity in ft/sec.
- Q = discharge in cfs.
- A = cross-sectional area in flow in ft^2
- R = hydraulic radius in ft.
- n = Manning's roughness coefficient in $ft^{-1/3}$ sec.
- S = slope of the energy line

From equation B2 it is apparent that the flow capacity of the pipe is proportional to the section factor $AR^{2/3}$ which, in turn, depends upon the diameter of the pipe and the ratio of the depth of flow to the pipe diameter. Figure 20 shows the relationship of the flow area A and the section factor $AR^{2/3}$ to the depth ratio d/D. The section factor has a maximum value of $0.38D^{8/3}$ at d/D = 0.94. That is for a given slope S the maximum flow capacity occurs when the pipe flows 0.94D full, D being the diameter of the pipe. However, when flow within the pipe is super-critical, as in this case, consideration must also be given to the possibility of cavitation and surging from flow instability or air entrainment. These factors may require that the grade of the pipe be reduced and/or the flow depth be reduced below the optimum obtained from discharge considerations alone.

The slope of the pipeline depends principally on the topography of the site. For the case under consideration the slope of the pipeline is approximately 0.10 as shown on Figure 18. The Manning's roughness coefficient depends on the material; for steel pipes n may vary from 0.010 to 0.017 whilst for concrete pipes it may vary between 0.010 and 0.020 (Chow 1959).

Pipe diameters required for various flow conditions within the pipe have been computed from Manning's equation using the two limiting values of n of 0.01 and 0.02. Results are given in Table 3.1.

Table 3.1: Required Pipe Diameters for Various Flow Conditions

$$Q = \frac{1.49}{n} AR^{2/3} S^{1/2}$$

Q = 200 cfs, S = 0.10

$\frac{d}{D}$	$\frac{AR^{2/3}}{D^{8/3}}$	$\frac{A}{D^2}$	n = 0.010			n = 0.020		
			$AR^{2/3} = 4.25$			$AR^{2/3} = 8.50$		
			D (ft.)	A (ft^2)	$V = \frac{Q}{A}$ (ft/sec)	D (ft)	A (ft^2)	$V = \frac{Q}{A}$ (ft/sec)
0.6	0.210	0.50	3.09	4.78	41.9	4.01	8.04	24.9
0.7	0.260	0.58	2.85	4.70	42.6	3.70	7.82	25.6
0.8	0.305	0.68	2.68	4.89	41.0	3.49	8.30	24.1
0.9	0.332	0.75	2.60	5.07	39.5	3.38	8.58	23.5
0.94	0.335	0.77	2.59	5.19	38.5	3.36	8.70	23.4

Table 3.1 can be used to obtain pipe diameters for any selected design criteria. If a depth ratio of 0.8 and a Manning's n value of 0.02 is chosen, the required pipe diameter is 3.49 ft. and the corresponding velocity is 24.1 f.p.s. at the design discharge.

For high velocity flows one of the main design considerations is the velocity that can be tolerated without danger of cavitation erosion. The allowable velocity will depend on the material used for construction. D. Colgate (1959) reported that incipient cavitation on a concrete surface was closely related to the flow depth, average velocity and the average height of the exposed aggregate above the surface. The results of Colgate's studies are given in Figure 28.

At the design discharge flow velocities can be obtained from Table 3.1. However, it should be noted that higher velocities may result at discharges less than the design discharge. For a given Manning's roughness coefficient n and slope S the velocity of flow within the pipe is proportional to the two-third power of the hydraulic radius. From Figure 20 it can be seen that $R^{2/3}$ has its maximum value of $0.45D^{2/3}$ corresponding to a depth ratio, d/D, of approximately 0.8. Another factor to be considered is the factor of safety used in choosing the value of n for design. For example, if a value of 0.020 is used, Table 3.1 shows that for a depth ratio of d/D of 0.8 a 3.49 ft. diameter pipe would be required and the velocity of flow would be 24.1 f.p.s. at the design discharge. Should the actual roughness be only 0.01 then Figure 20 shows that the actual

flow depth would be only 0.49D and the actual velocity would be as high as 42.5 f.p.s.

From the above considerations it is estimated that the flow velocities in the high velocity flume could range between 20 and 50 f.p.s. Figure 28 indicates that under these conditions cavitation damage is unlikely to occur provided the surface is smooth.

Flow stability is a further condition that must be considered in the design of pipes carrying high velocity flow. Escoffier and Boyd (1962) have shown that for supercritical flow in a pipe flowing partially full, the flow may be steady or pulsating, depending on the depth ratio d/D and a parameter J defined by the expression:-

$$J = \frac{S^{\frac{1}{2}} \, D^{1/6}}{n}$$

where S = slope of pipeline
D = diameter of pipe in ft.
n = Manning's roughness coefficient in sec. $ft.^{-1/3}$

The type of flow as a function of the parameter J and the depth ratio $\frac{d}{D}$ is shown in Figure 29. In the case under consideration, the J-value is about 20, and the flow is in the steady rapid flow, when the depth ratio is about 0.7.

As the pipe is laid on a steep slope, air-entrainment will occur. As a result of the entrained air that will be carried away together with the flow, an adequate supply of air is needed to maintain atmospheric pressure in the pipe. The air entrained into the flow affects the bulk of flow. The insufflation of air increases the volume of flow and hence it will have a greater depth than for pure water. The quantity of entrained air has been estimated at about 0.1 of the water discharge (Straub and Anderson, 1960).

In this investigation, a Manning's n value of 0.020 is assumed, and a pipe diameter of 3.75 ft. is used. Under these conditions, for the design discharge of 200 c.f.s. the pipe is flowing at a depth ratio of 0.68D, or a depth of 2.55 ft. and the velocity of the flow is 25.2 ft/sec., which is considered to be safe against cavitation erosion from the previous discussion.

At a depth of 0.68D for the clear water flow, the cross-sectional area of the flow is $0.57D^2$, or 8 $ft.^2$ (See Fig. 20). If the entrained air is taken as 0.1 of the water flow, the cross-sectional area of the water-air mixed flow will be increased by 10 per cent compared with that of the pure water flow, that is, 8.8 $ft.^2$ or $0.63D^2$. From Fig. 20 it can be seen that the water-air mixture will be flowing at a depth ratio of 0.75.

Appendix C: Computation of Depth-Discharge Relations for Free Surface Flow.

When the flow in the inlet transition has a free surface, the flow profile is controlled by the critical depth at the break of grade of the bed of the approach channel and the invert slope of the transition. The critical depth for a given discharge can be computed from Equation C1, that is

$$\frac{Q^2 T}{gA_c^3} = 1 \qquad \text{C1}$$

where Q = discharge in c.f.s.
T = surface width of flow in ft. = $D \sin \theta/2$
A_c = cross-sectional area of flow in ft^2
$= D^2/8 \, (\pi \theta/180 - \sin \theta)$
D = diameter of pipe at throat in ft.
θ = included angle as defined in Fig. 19 in degrees.

When $D = 5.17$ ft., and $g = 32.2$ ft/sec^2, Equation (24) can be rewritten as

$$\frac{\sin \frac{\theta}{2}}{\left(\frac{\pi}{180} \theta - \sin \theta\right)^3} = \frac{gD^5}{512 Q^2} = \frac{232}{Q^2} \qquad \text{C2}$$

For any given value of Q, equation C2 can be solved for θ and the critical depth and the cross-section area of the flow can be obtained with the aid of Fig. 20.

Neglecting friction the Bernoulli equation can be written between the inlet and a section upstream in the approach channel, as

$$d_c \cos \alpha + \frac{V_c^2}{2g} = H + \frac{V^2}{2g}$$

where d_c = critical depth at inlet in ft.
α = angle of inclination of the invert of the inlet transition
V_c = critical velocity at inlet in ft/sec.
H = depth of flow in approach channel in ft.
V = approach velocity of flow in channel where H is measured, in ft/sec.

The computations are shown in Table 3.2 for an angle of inclination of 45° as used for the inlet designed and tested, and the results are plotted in Figure 27.

Table 3.2: Computation of the Free Surface Flow Depth-Discharge Curve.

Q cfs (1)	$\frac{232}{Q^2}$ (2)	θ degrees (3)	$\frac{d}{D}$ (4)	$d=Dx(4)$ (ft) (5)	$d\cos\alpha = 0.707d$ (ft) (6)	A_c (ft^2) (7)
90	0.0284	184°	0.51	2.64	1.86	10.8
120	0.0160	203°	0.63	3.25	2.30	13.9
150	0.0102	221°	0.67	3.46	2.45	15.0
180	0.0071	237°	0.745	3.85	2.72	16.7
210	0.0052	253°	0.79	4.08	2.88	17.8
240	0.0040	265°	0.84	4.33	3.06	18.7
270	0.0032	280°	0.88	4.55	3.22	19.5
300	0.0026	290°	0.91	4.70	3.32	20.0

v_c (8)	$\frac{v_c^2}{2g}$ (9)	$H = (6)+(9)$ (10)	$A_{channel} = (6+1.5H)H$ (11)	v (12)	$\frac{v^2}{2g}$ (13)	Corrected $H = (10)-(13)$ (14)
8.3	1.08	2.94	30.6	2.94	0.13	2.81
8.6	1.15	3.45	38.6	3.11	0.15	3.30
10.0	1.55	4.00	48.0	3.12	0.15	3.85
10.8	1.80	4.52	57.8	3.12	0.15	4.37
11.8	2.16	5.04	68.2	3.08	0.15	4.89
12.8	2.55	5.62	81.2	2.96	0.14	5.48
13.8	2.97	6.19	94.5	2.86	0.13	6.06
15.0	3.50	6.82	110	2.72	0.12	6.70

Note: Column 10 assumes $\frac{v^2}{2g}$ small with respect to H.

Computation of Depth-Discharge Curve for Sluice Flow

When the inlet transition runs full and an air vent is provided at the junction of the inlet transition and the pipe, the flow in the pipe runs part full since air can be drawn in through the vent. The discharge in the pipe depends on the difference in level of the flow surface in the approach channel and the soffit of the pipe at the throat. Neglecting losses the Bernoulli equation can be written as -

$$H + Z = d_t + \frac{V_t^2}{2g}$$

where H = depth of flow in the channel in ft.
Z = difference in level of the approach channel bed and the invert of the pipe at the throat, in ft.
d_t = diameter of pipe at throat, in ft.
V_t = velocity of flow in throat, in ft/sec.

The computation of H for different Q values is shown in Table 3.3 and the results plotted in Fig. 27.

In the above computation, the loss through the inlet transition is neglected. This loss can be taken into consideration by inserting a discharge coefficient into the Bernoulli equation which becomes

$$H + Z = d_t + \frac{v_t^2}{2gC_d^2}$$

The value of C_d depends on the geometry of the inlet transition. In the case under consideration, the inlet transition just upstream of the throat is formed of a portion of a cone. The sides of the cone make an angle of about 6^o with the axis and the discharge coefficient can be estimated at 0.95, which is the value used for convergent short tubes of similar geometry (King's Handbook of Hydraulics, 1963).

The computation of the depth-discharge curve for sluice flow with loss taken into account is shown in Table 3.4 and the results are plotted in Figure 27.

Table 3.3: Computation of the Theoretical Sluice Flow Depth-Discharge Curve (Loss neglected)

d_t = 3.75 ft. (throat) $A_t = \frac{\pi}{4}(3.75)^2$ (throat) $= 11.06\ ft^2$ $V_t = \frac{Q}{A_t}$		$h_{vt} = \frac{V_t^2}{2g}$ $H + 6.50 = d_t + h_{vt}$ $H = d_t + h_{vt} - 6.50$ $= h_{vt} - 2.75$	
Q	V_t	$h_{vt} = \frac{V_t^2}{2g}$	$H = d_t + h_{vt} - 6.50$ $= h_{vt} - 2.75$
cfs	ft/sec.	ft.	ft.
(1)	(2)	(3)	(4)
150	13.6	2.85	0.10
180	16.3	4.12	1.37
210	19.0	5.60	2.85
240	21.7	7.31	4.56
270	24.4	9.26	6.51
300	27.2	11.45	8.70

Table 3.4: Computation of the Theoretical Sluice Flow Depth-Discharge Curve (Loss taken into account)

d_t = 3.75 ft. (throat) A_t = 11.08 ft^2 (throat) $V_t = \frac{Q}{A_t}$		C_d = 0.95 $h_{vt} = \frac{V_t^2}{2g\,C_d^2}$ $H = d_t + h_{vt} - 6.50$ $= h_{vt} - 2.75$	
Q cfs	V_t ft/sec.	$h_{vt} = \frac{V_t^2}{2gC_d^2}$ ft	$H = h_{vt} - 2.75$
(1)	(2)	(3)	(4)
150	13.6	3.16	0.41
180	16.3	4.56	1.81
210	19.0	6.20	3.45
240	21.7	8.10	5.35
270	24.4	10.25	7.50
300	27.2	12.70	9.95

References

(1) Babbitt, Doland and Cleasby "Water Supply Engineering" McGraw Hill Pub. 6th Ed. 1962, p. 426.

(2) Camp T.R. (1946) "Sedimentation and the Design of Settling Tanks" Trans. A.S.C.E. Vol. 111, 1946, p. 895.

(3) Dobbins, W.E. (1944) "Effect of Turbulence on Sedimentation" Trans. A.S.C.E. Vol. 109, 1944, p. 629.

(4) Ewers and Stone (1965) "Size of materials taken from the bed of the Hunter River at Site 2 - Parry's Property, and Site 3 - Jerry's Plains" Uni. N.S.W. Water Research Laboratory Progress Report No. 1 Project E. 888, Jan. 1965.

(5) Foster, D.N. "Laboratory study of design procedures for stability of rock lined channel against flow and waves" Uni. N.S.W. Water Research Laboratory Progress Report No. 2 Porject E. 894, March, 1966.

(6) Hazen A. (1904) "On Sedimentation" Trans. A.S.C.E. Vol. L111, 1904 p. 63.

(7) Miller, D.G. (1964) "Sedimentation - A Review of Published Work" Water and Water Eng. Feb. 1964 p. 52.

(8) Richardson, J.F. et al (1961) "Sedimentation and Fluidisation" Trans. Instn. Chem. Engr. 1954, 32, 35; 1958, 36, 270; 1961, 39, 348; 1961, 39, 357.

(9) Rouse H. (1949) "Engineering Hydraulics" John Wiley and Sons Publ. 1949.

(10) Chow, V.T. "Open Channel Hydraulics", McGraw-Hill, 1959, p. 110.

(11) Colgate D., "Cavitation Damage of Roughened Concrete Surface" Proceedings, A.S.C.E. Vol. 85 No. HY 11, Nov. 1959.

(12) Escoffier, F.F., and Boyd M.B., "Stability Aspects of Flow in Open Channels". Proceedings, A.S.C.E. Vol. 88 No. HY 6, Nov. 1962.

(13) Staub, L.G., and Anderson, A.G., "Self-Aerated Flow in Open Channels", Transactions, A.S.C.E., Vol. 125, 1960.

(14) King, H.W., and Brater, E.F., "Handbook of Hydraulics" McGraw-Hill, 5th Ed., 1963.

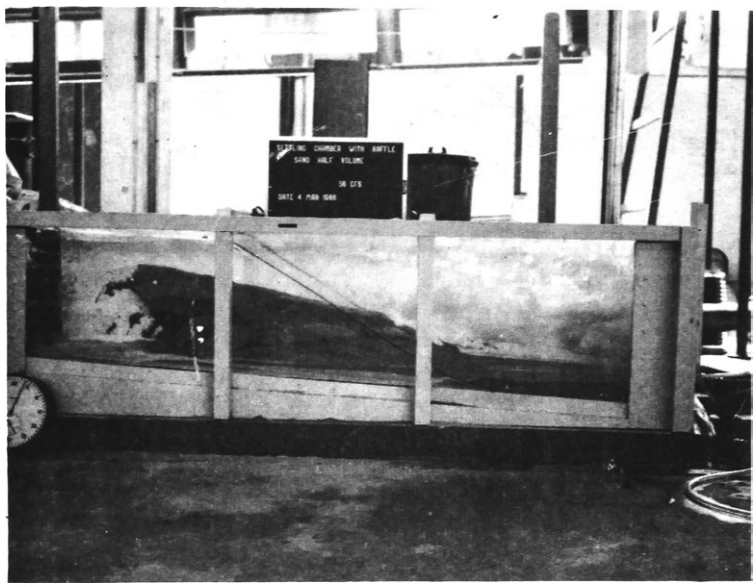

Fig. 1: Hanging up of sand on side walls during flushing period. (With baffle).

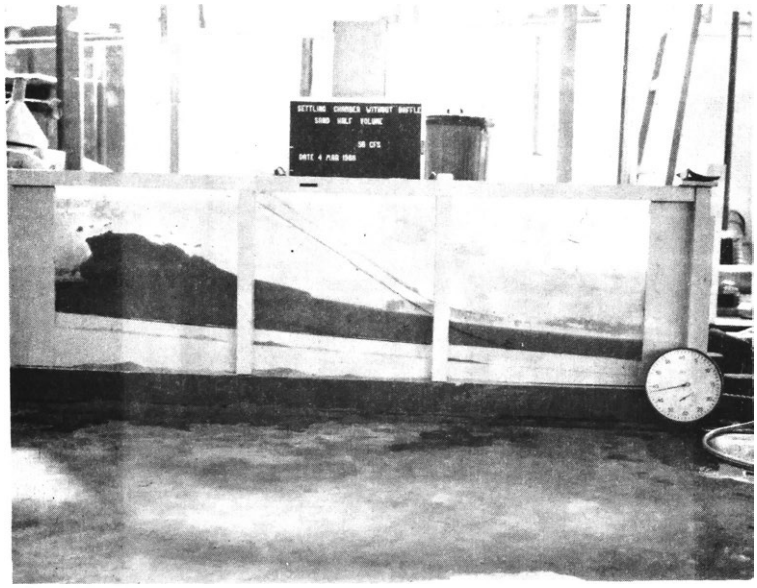

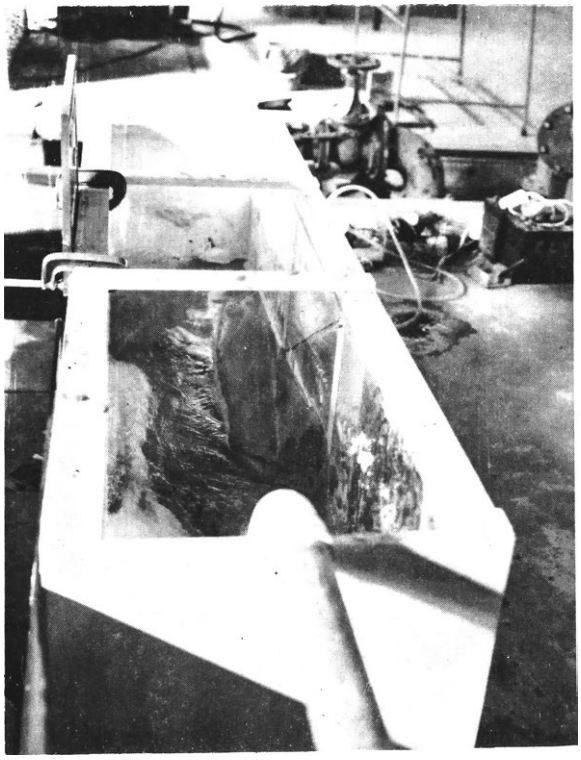

Fig. 2: Hanging up of sand on side walls during flushing period. (No baffle).

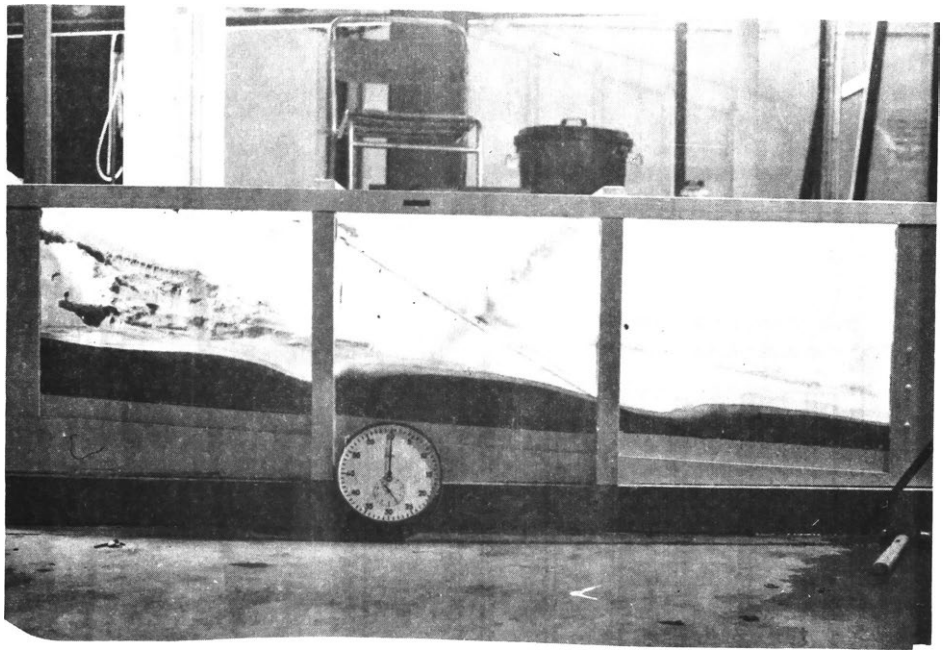

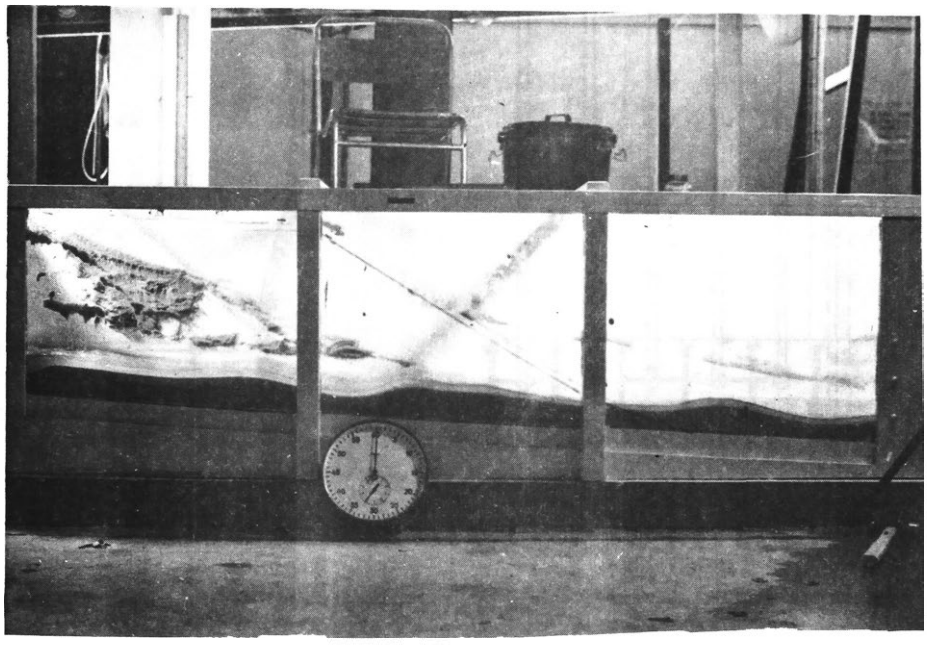

Fig. 3: Dune formation during scour.

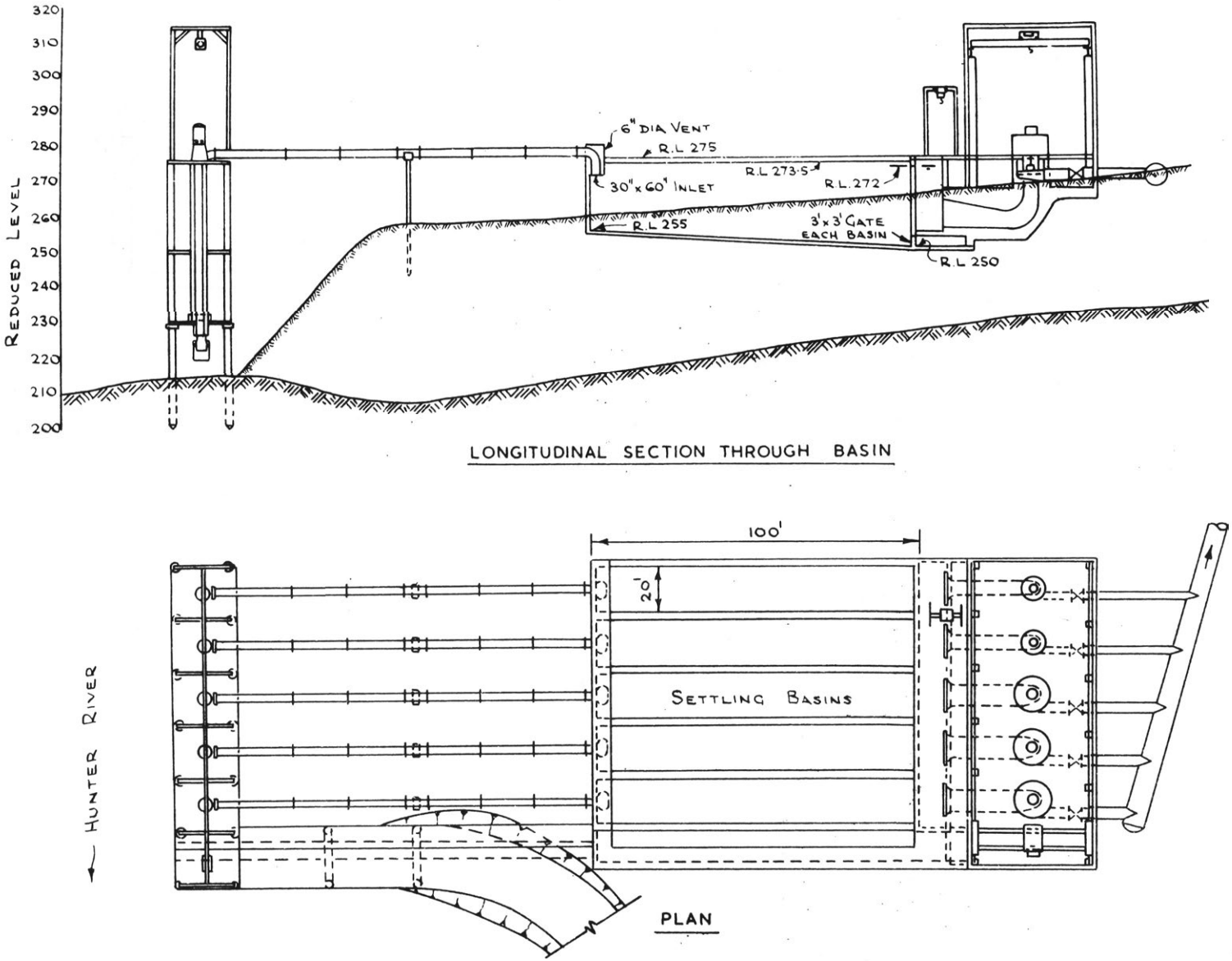

FIGURE 4: SETTLING CHAMBER - Preliminary Proposal

CE-E-6678

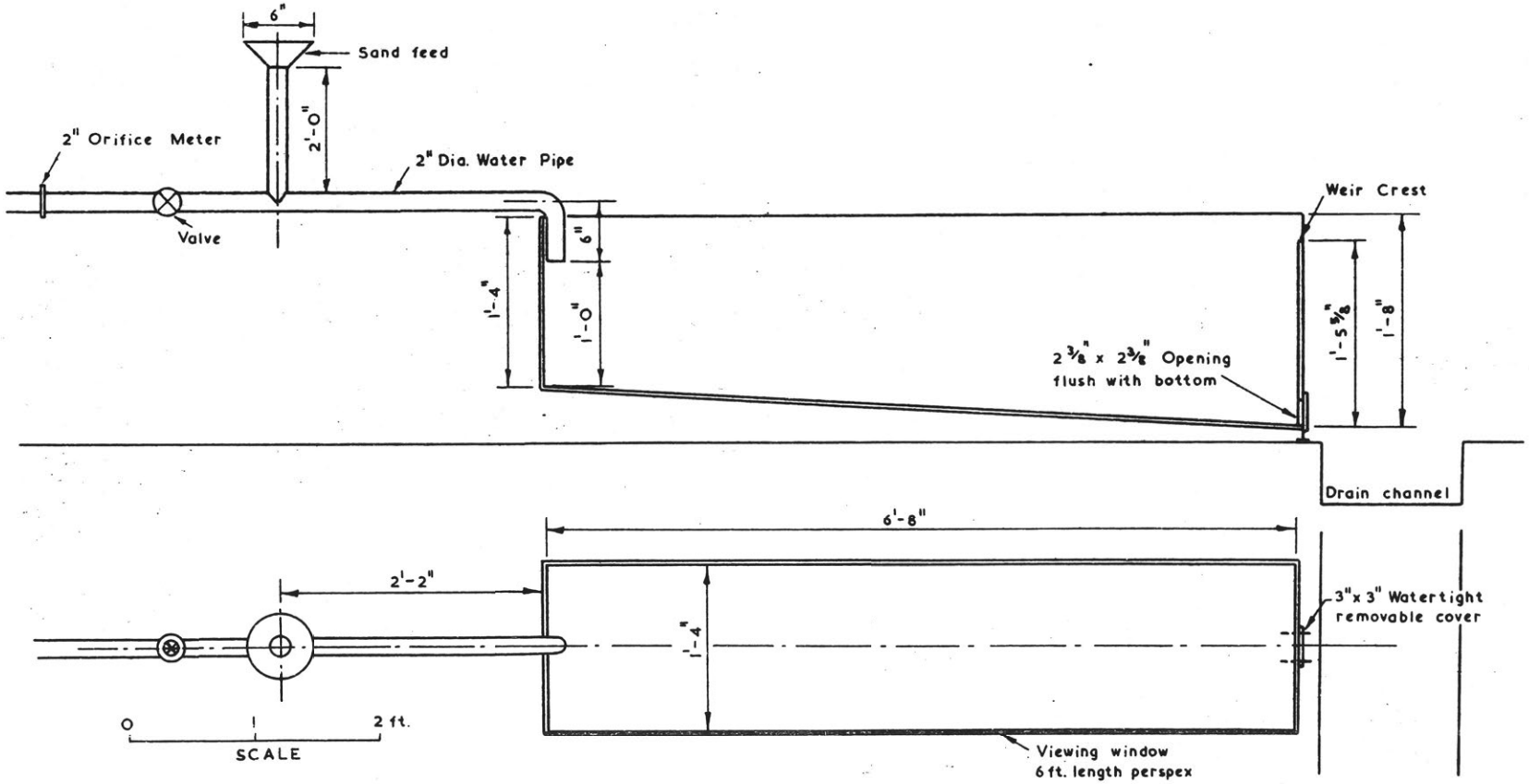

FIGURE 5: SETTLING TANK - MODEL DETAILS

CE-E-6679

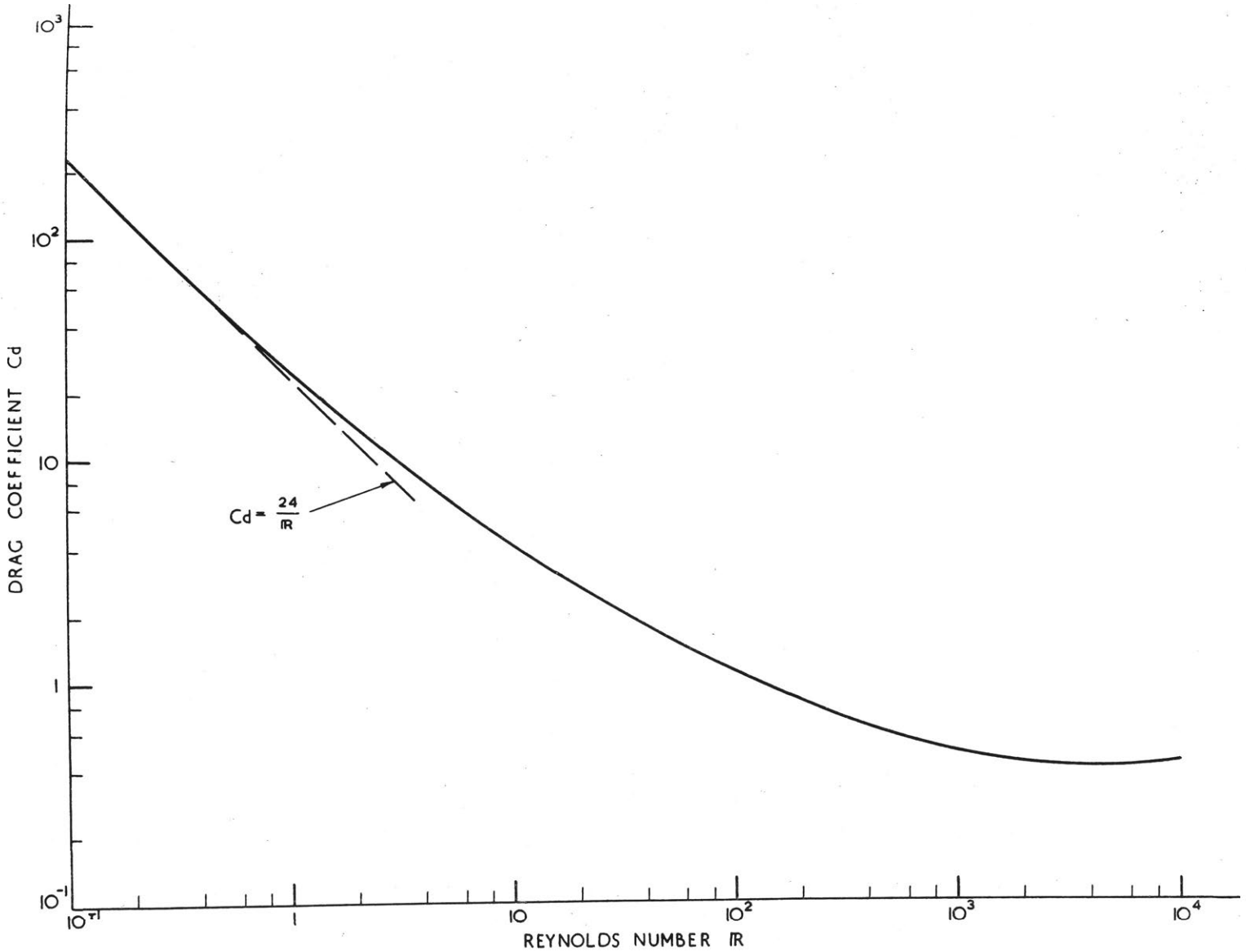

FIGURE 6: DRAG COEFFICIENT AS A FUNCTION OF REYNOLDS NUMBER

(AFTER ROUSE 1949, p. 122)

CE-E-7933

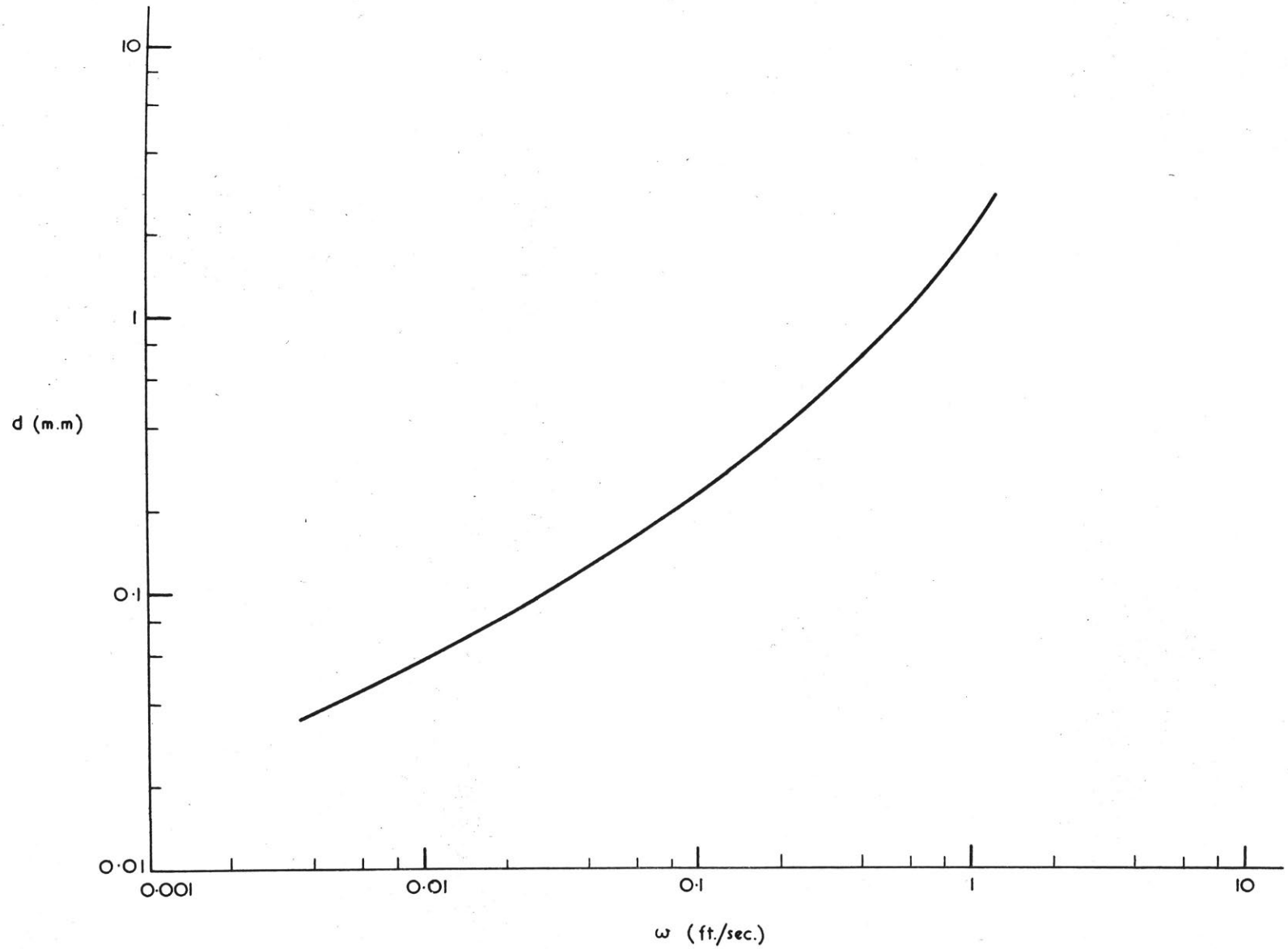

FIGURE 7: SETTLING VELOCITIES OF QUARTZ SPHERES
(SPECIFIC GRAVITY = 2·65, TEMPERATURE = 70° F.)

CE-E-7934

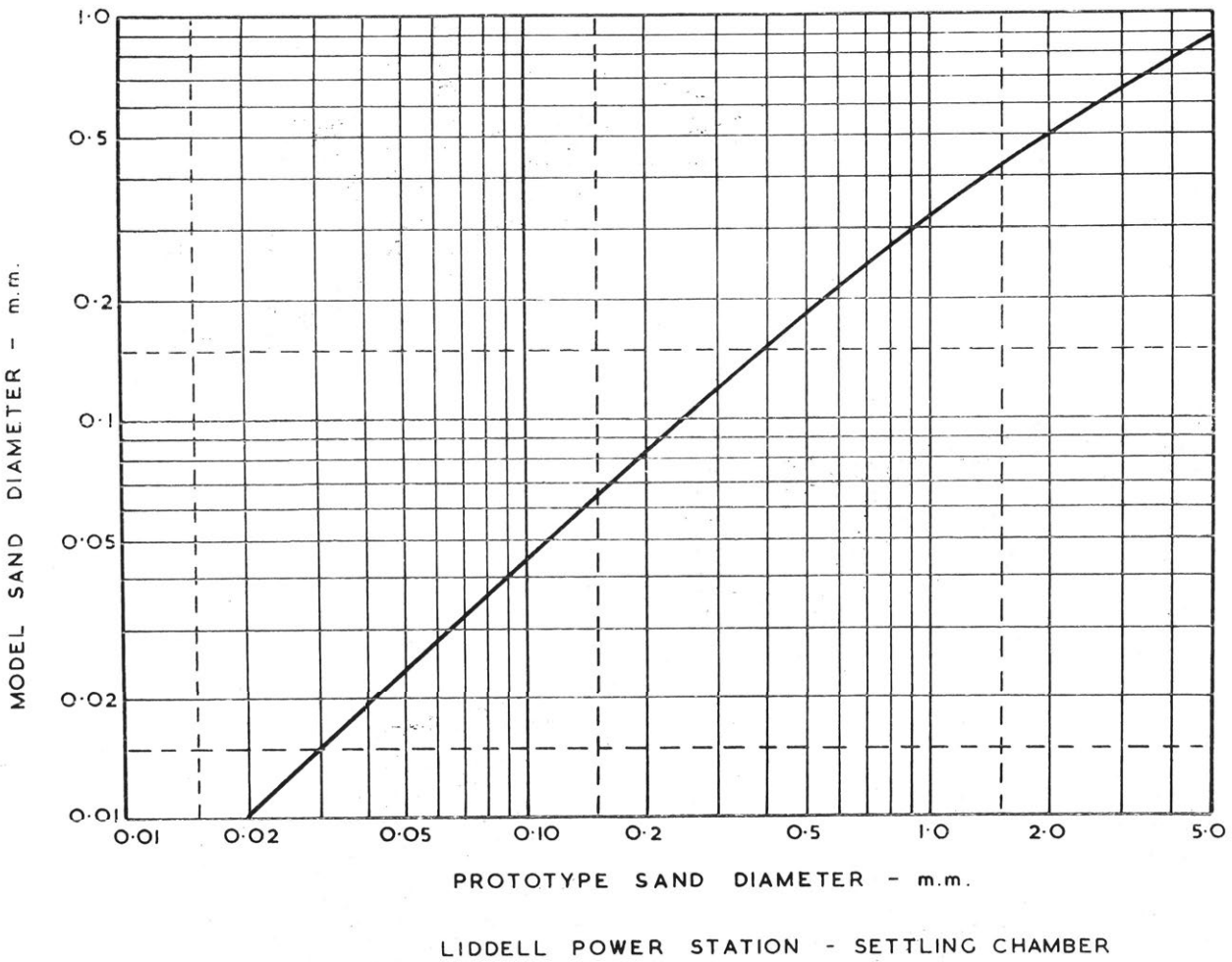

FIGURE 8: RELATIONSHIP BETWEEN MODEL & PROTOTYPE SAND SIZES
(Model Scale 1:15 Temperature 70° F.)

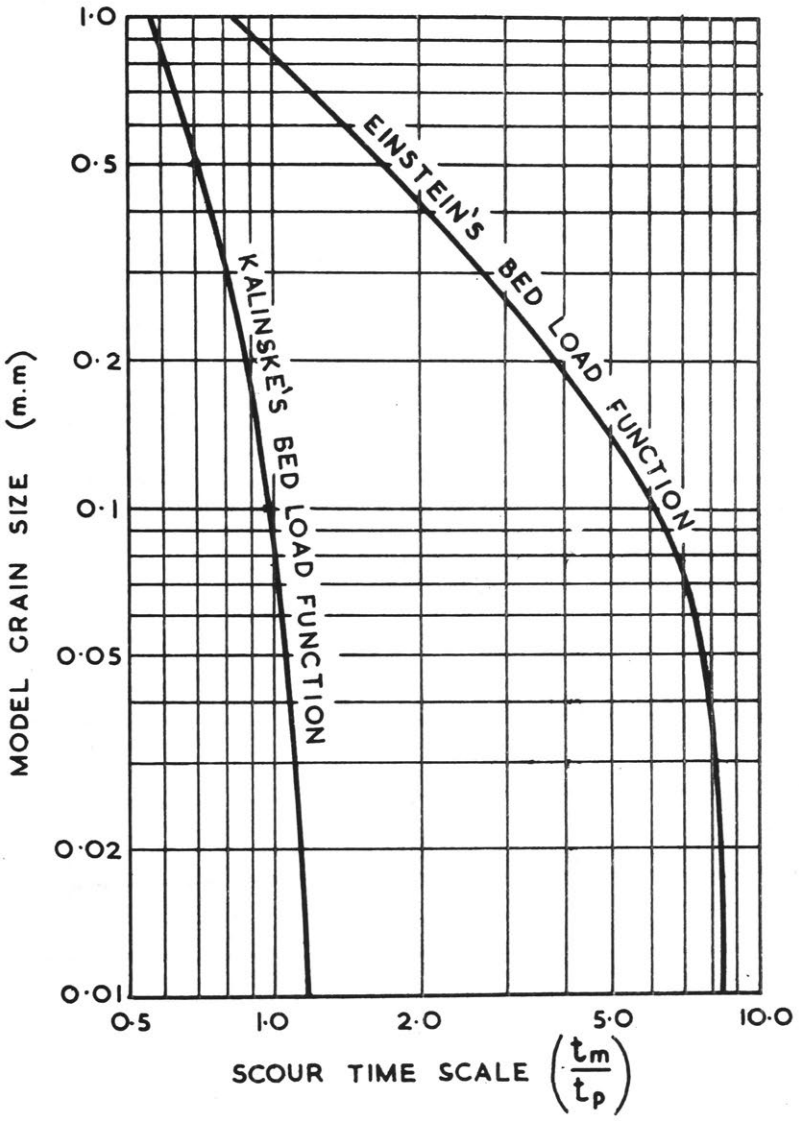

FIGURE 9: SCOUR TIME SCALES FOR VARIOUS MODEL SAND SIZES - MODEL SCALE 1:15

CE-E-6682

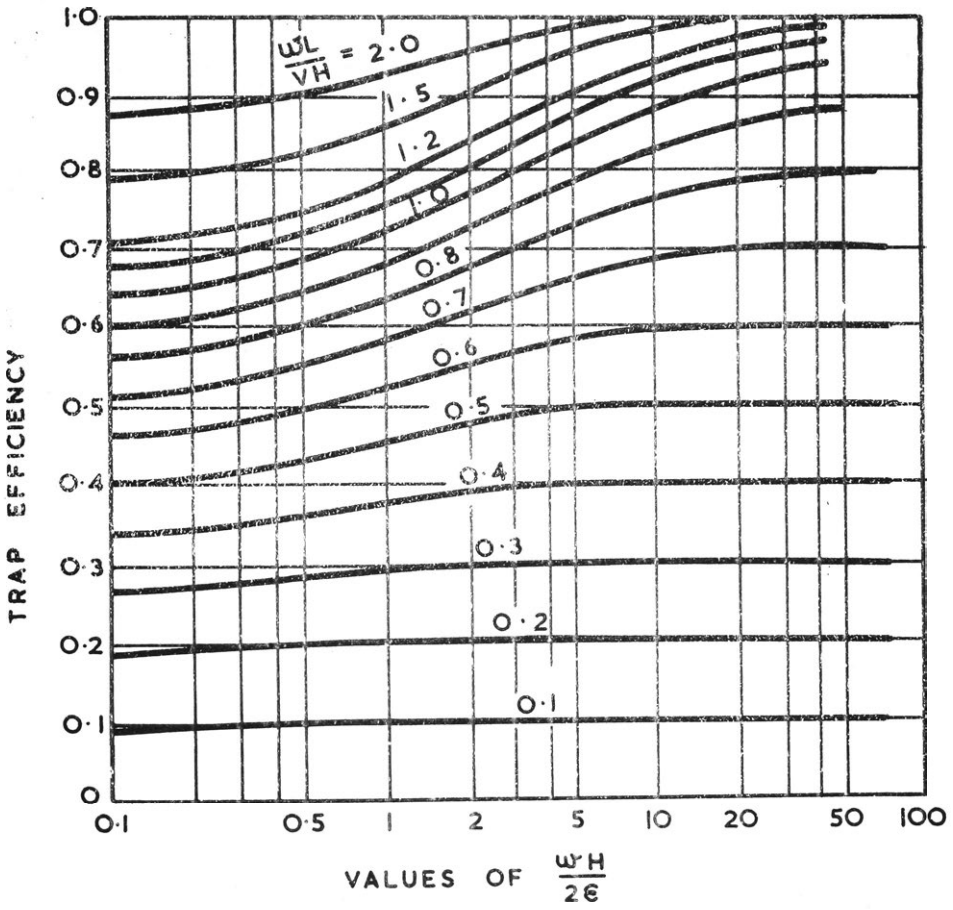

FIGURE 10: TRAP EFFICIENCY OF SETTLING BASINS

(AFTER CAMP 1946)

CE-E-6683

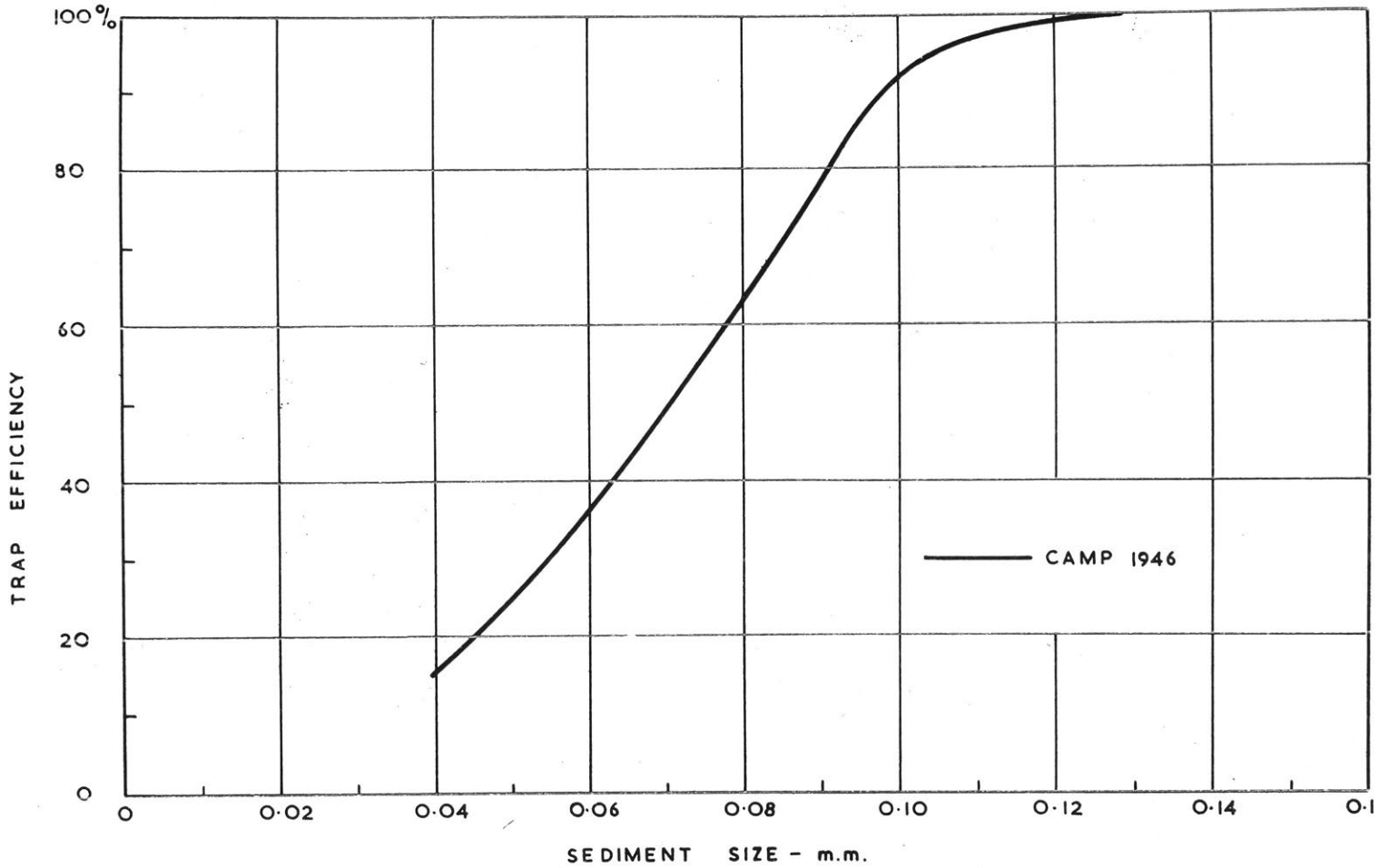

FIGURE II: TRAP EFFICIENCIES OF BASIN
(After Camp 1946)

CE-E-6684

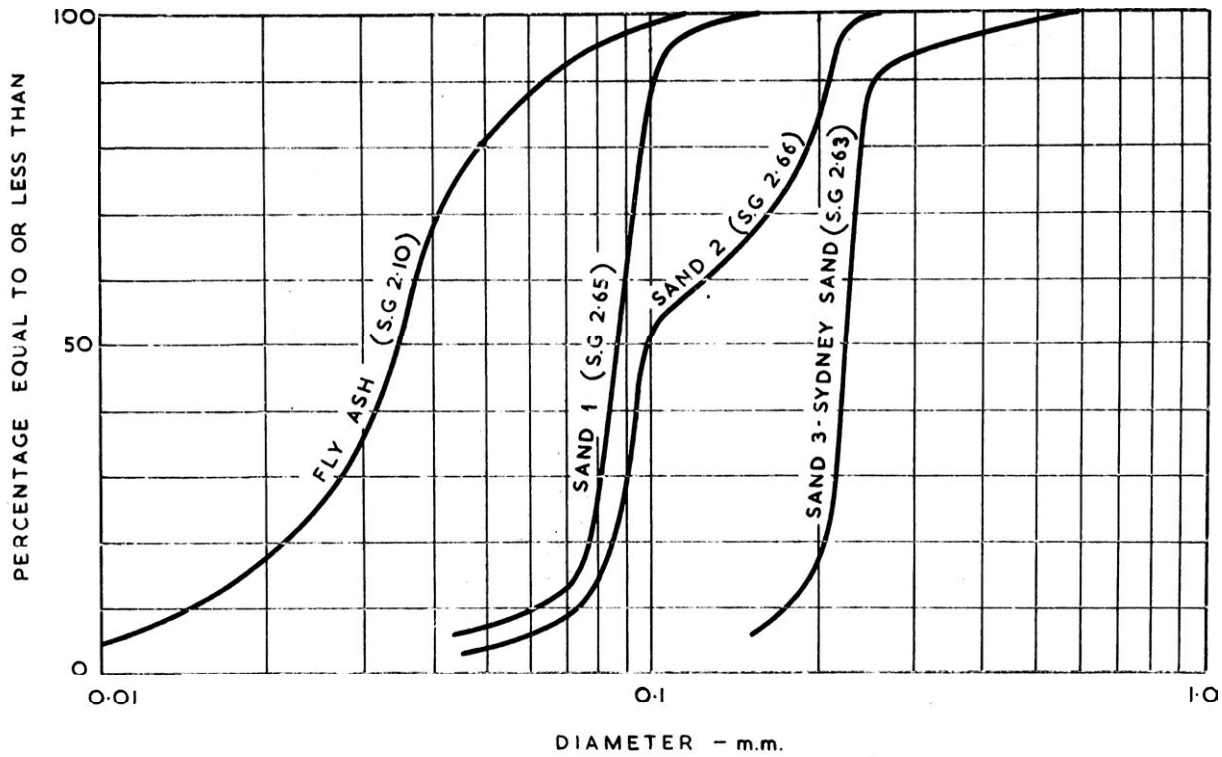

FIGURE 12: SIZE GRADINGS OF MODEL SEDIMENTS

CE-E-6685

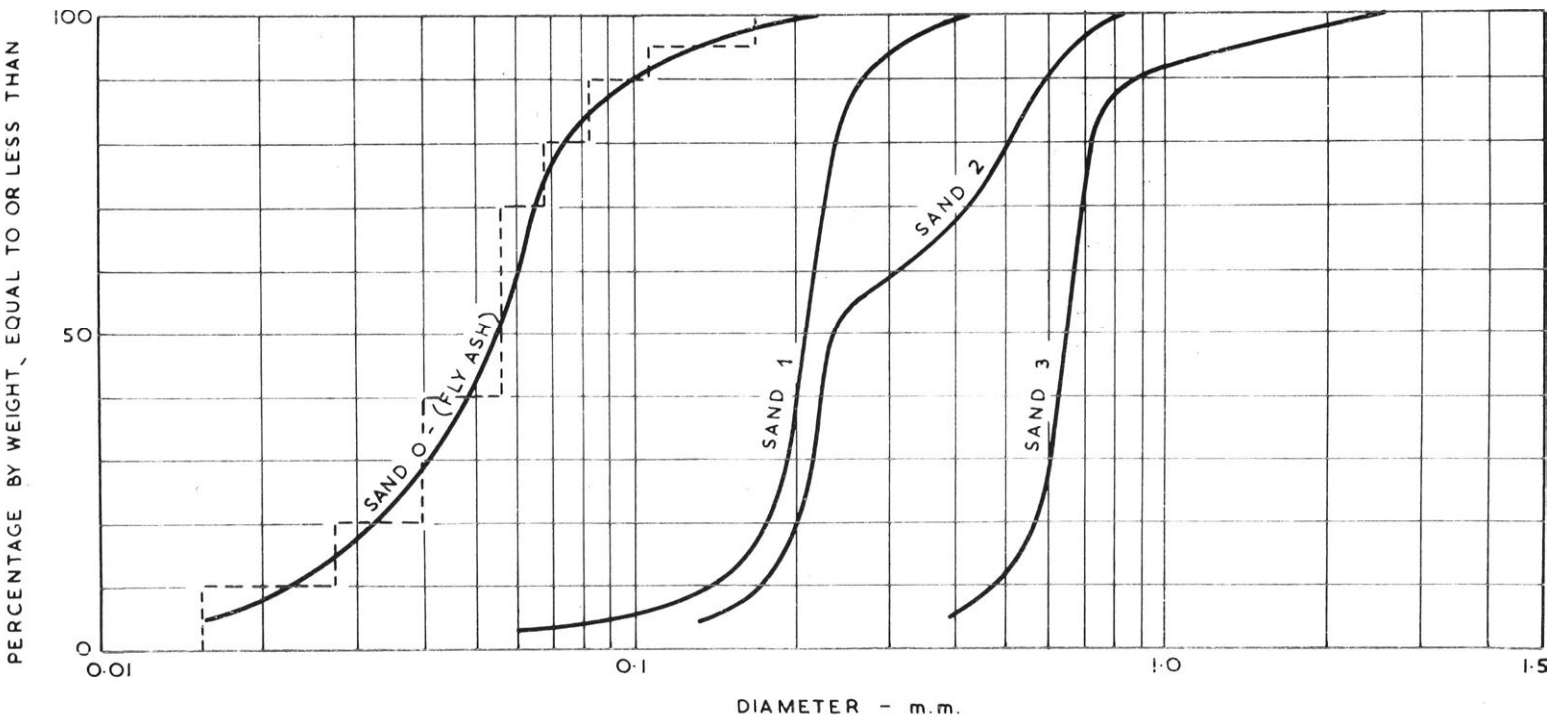

FIGURE 13 : EQUIVALENT SIZE GRADINGS OF PROTOTYPE SANDS (S.G 2·65) CORRESPONDING TO MODEL TEST SEDIMENTS

CE - E - 6686

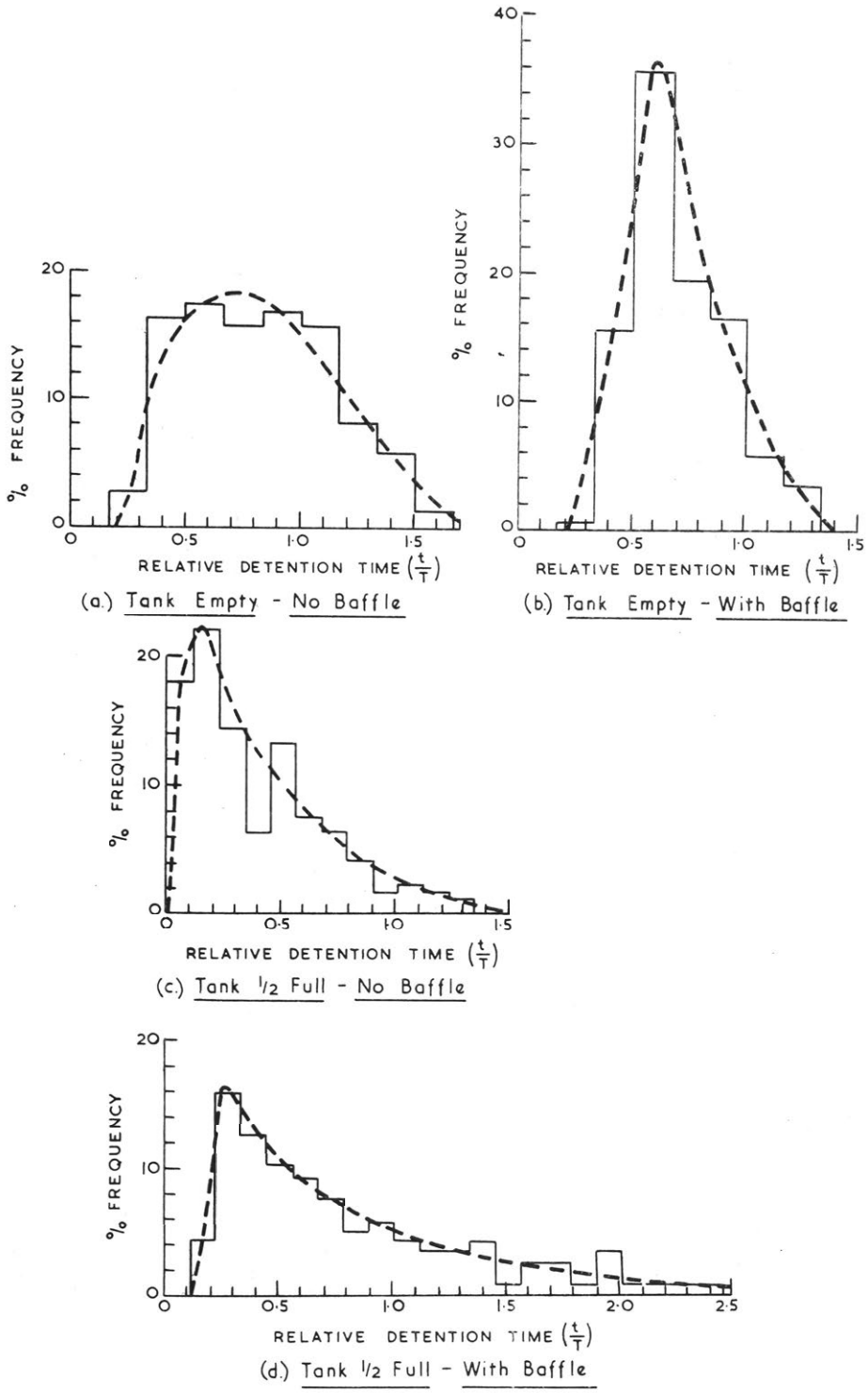

FIGURE 14: FREQUENCY DISTRIBUTIONS OF TANK DETENTION TIMES

CE-E-6687

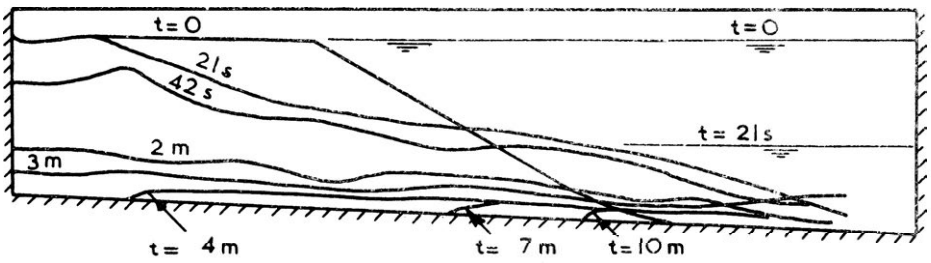

(a) WITHOUT INLET BAFFLE

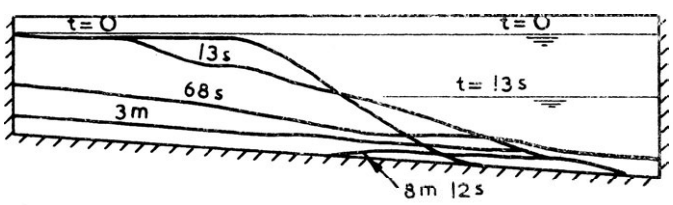

(b) WITH INLET BAFFLE

FIGURE 15: PROFILES OF SAND BED AT VARIOUS TIMES AFTER OPENING OF SCOUR VALVE

(Times ave. to Model Scale)

CE-E-6688

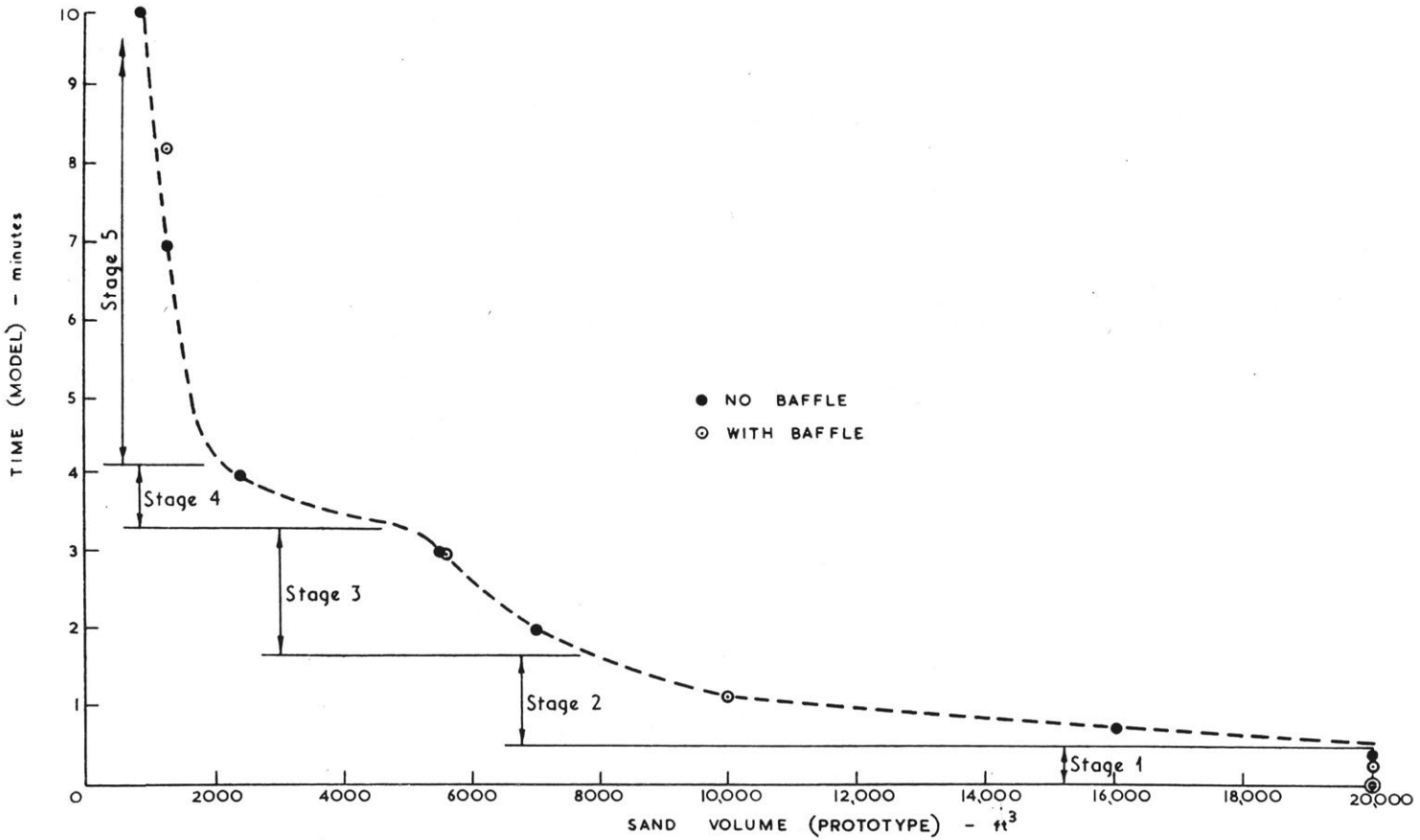

FIGURE 16: RATE OF CHANGE OF SAND VOLUME DURING FLUSHING OF SETTLING CHAMBER FROM HALF FILLED CONDITION

CE-E-6689

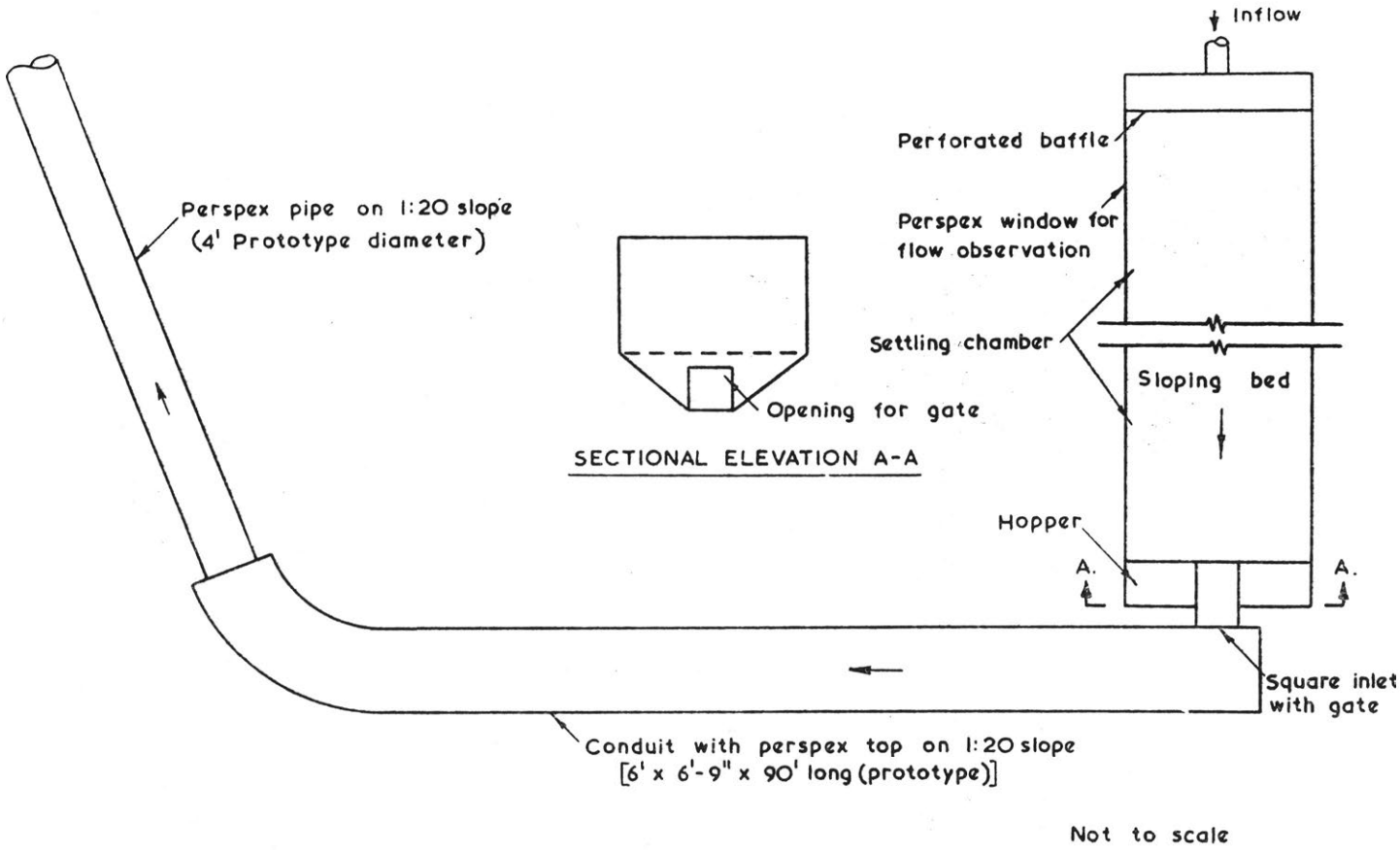

FIGURE 17: SKETCH OF GENERAL LAYOUT OF MODEL OF WASTEWAY FOR SETTLING CHAMBER

CE-E-6816

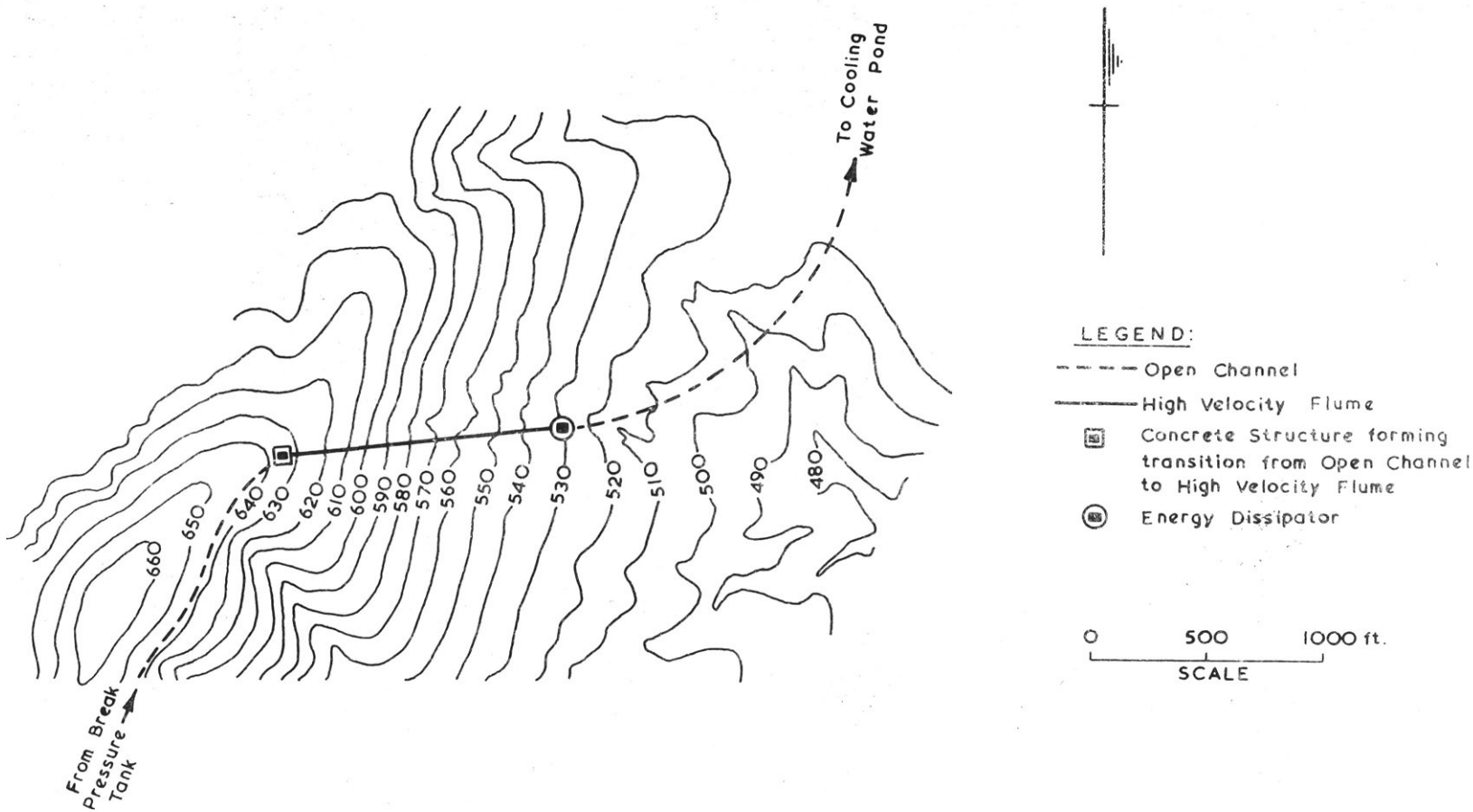

FIGURE 18: PROPOSED PIPELINE FOR LIDDELL P.S WATER SUPPLY SYSTEM

(After Fig. 17. Research Note No. 50. The Electricity Commission of N.S.W. Generation Investigation Section, Projects Division.) CE-E-6754

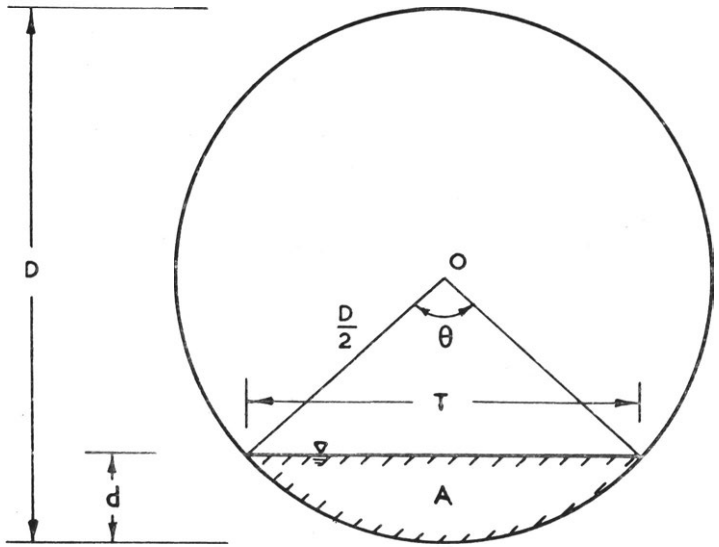

LEGEND

(1) Diameter of Pipe, D

(2) Included Angle, θ, in degrees

(3) Depth of Flow, d

$$d=\frac{D}{2}\left(1-\cos\frac{\theta}{2}\right)$$

(4) Flow Surface Width

$$T = D \sin\frac{\theta}{2}$$

(5) Flow Area

$$A=\frac{D^2}{8}\left(\frac{\pi}{180}\theta-\sin\theta\right)$$

(6) Wetted Perimeter

$$P=\frac{\pi}{360}\theta D$$

(7) Hydraulic Radius

$$R=\frac{A}{P}$$

FIGURE 19: DEFINITION SKETCH FOR FIG. 20 CE-E-6755

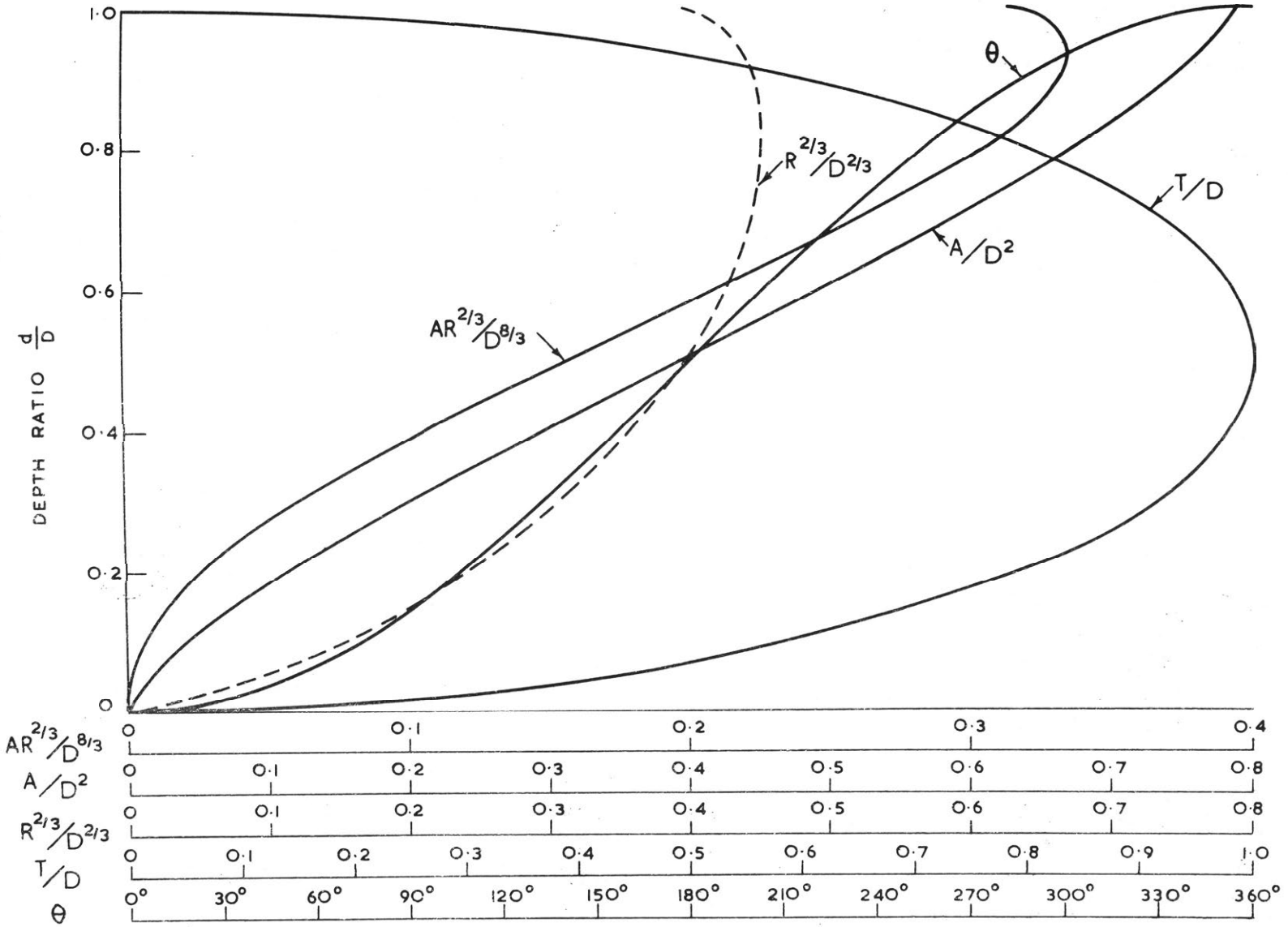

FIGURE 20: RELATIONSHIP OF SOME HYDRAULIC PARAMETERS TO DEPTH RATIO CE-E-6756

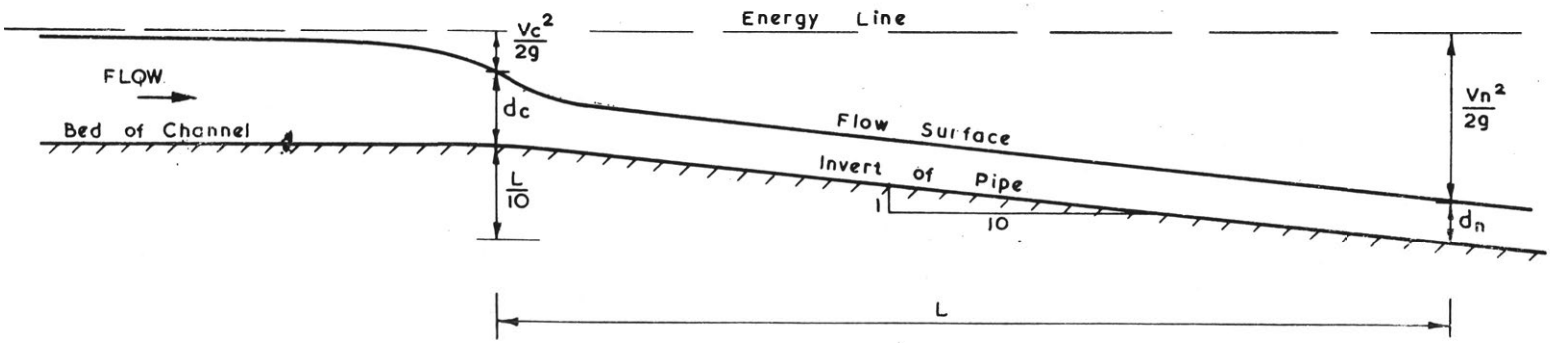

FIGURE 21: ENERGY RELATIONSHIP NEAR PIPE INLET TRANSITION CE-E-6757

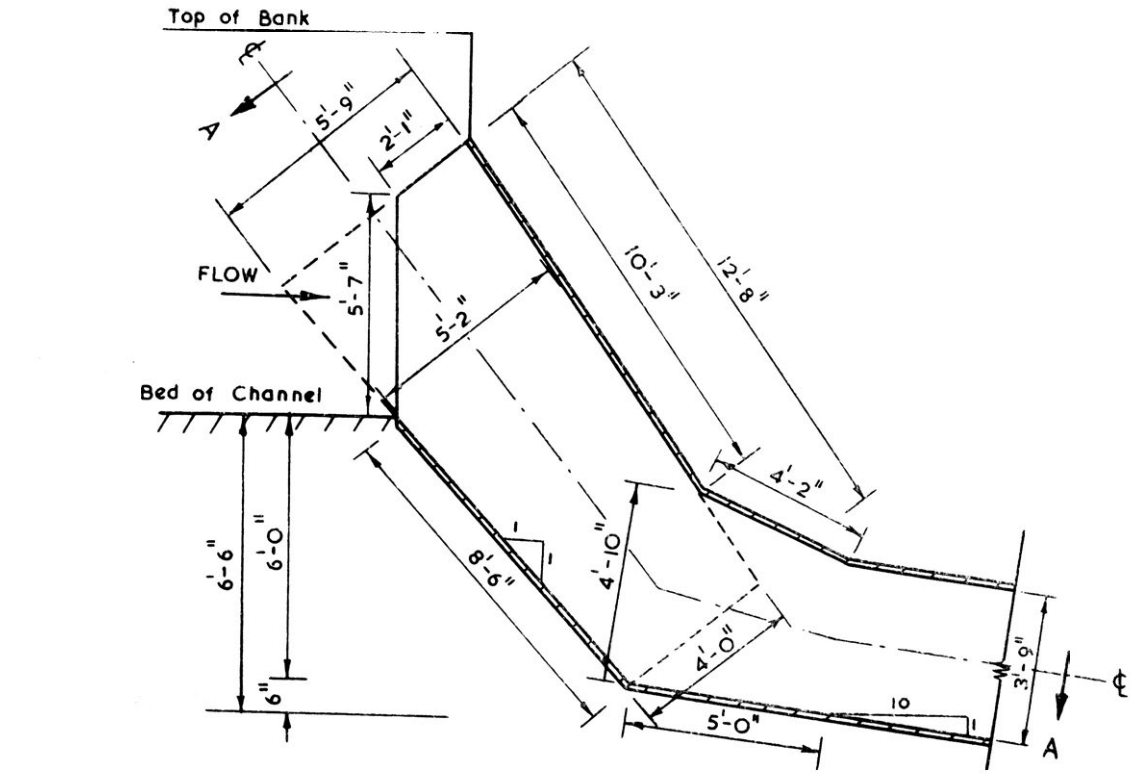

LONGITUDINAL SECTION

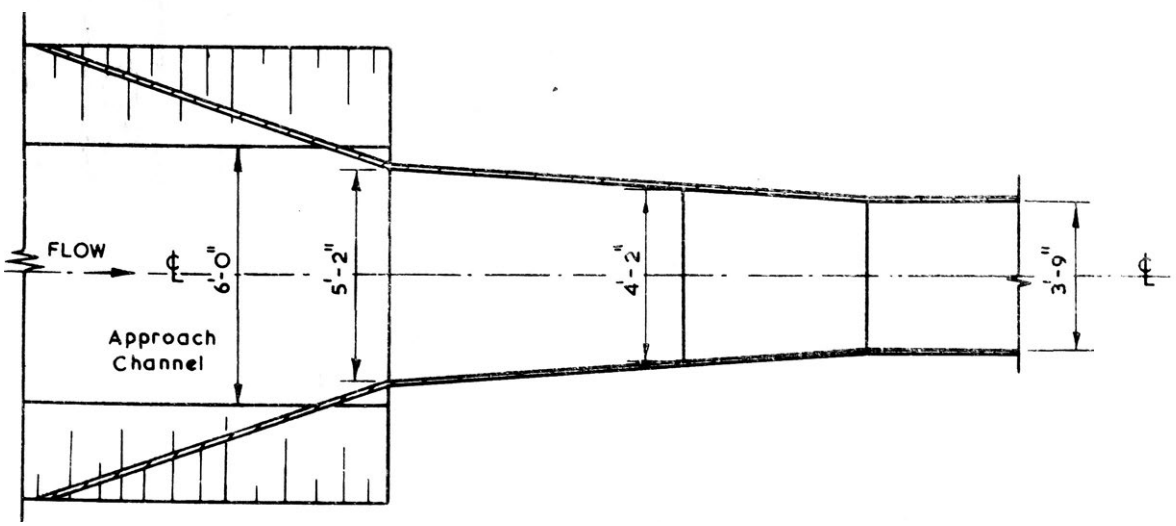

SECTION A-A (DEVELOPED ALONG ℄)

FIGURE 22: DETAIL OF PROPOSED PIPE INLET TRANSITION

CE-E-6758

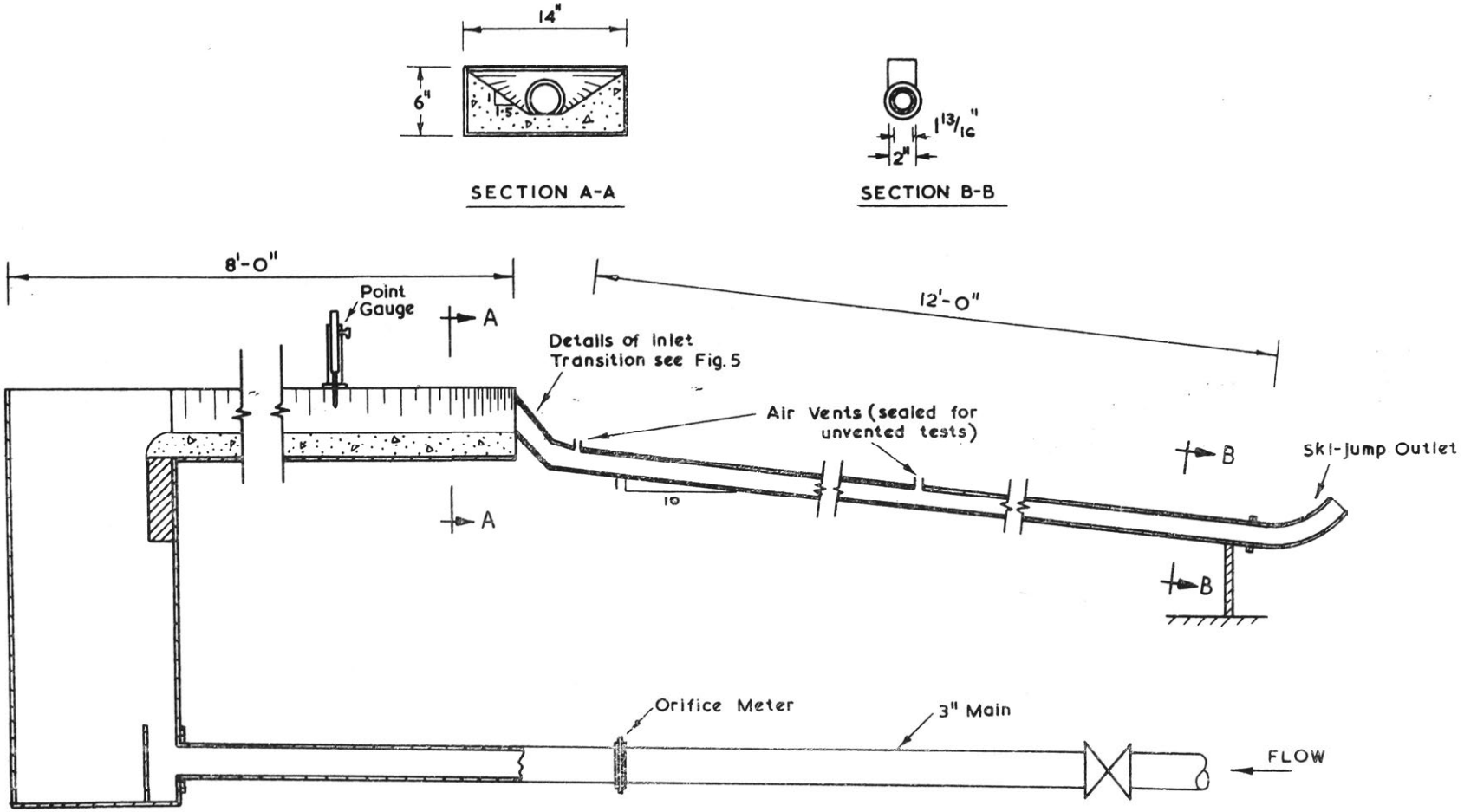

FIGURE 23: GENERAL LAYOUT OF PIPE INLET TRANSITION MODEL CE-E-6759

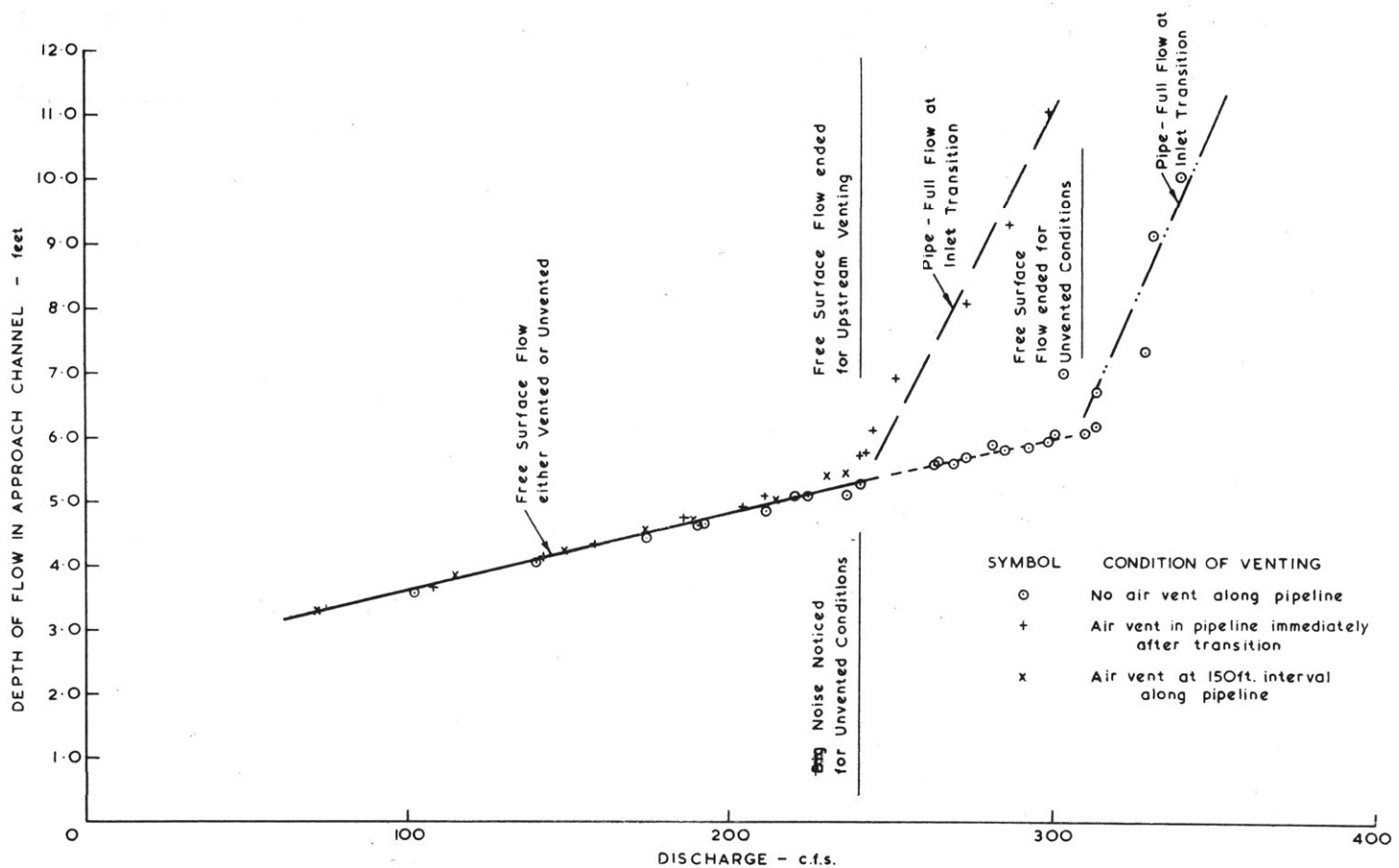

FIGURE 24: CHARACTERISTICS OF FLOW IN PIPELINE WITH DIFFERENT DEGREE OF VENTING CE-E-6760

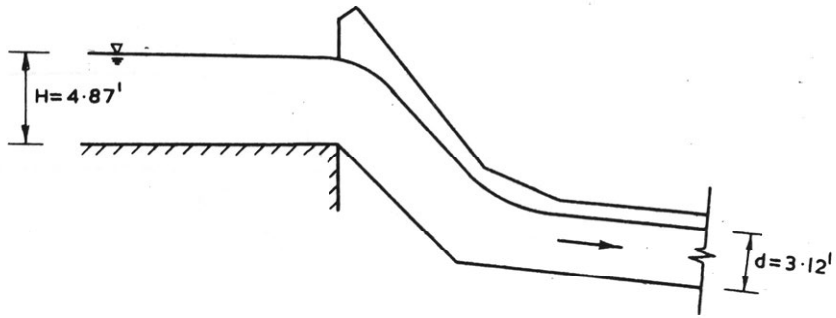

(a) Q=210 c.f.s. FREE SURFACE FLOW

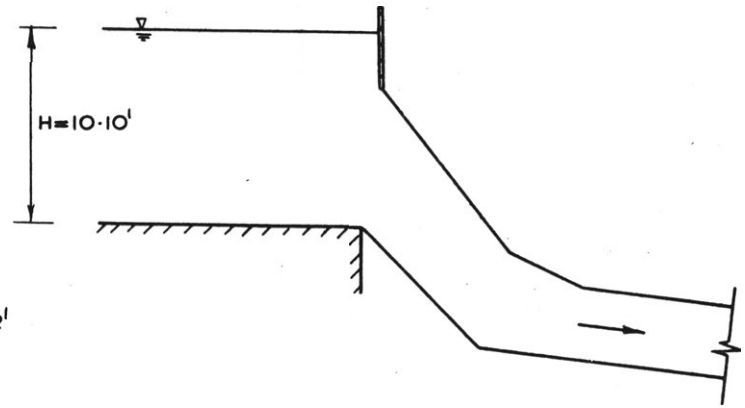

(c) Q=340 c.f.s. PIPE-FULL FLOW

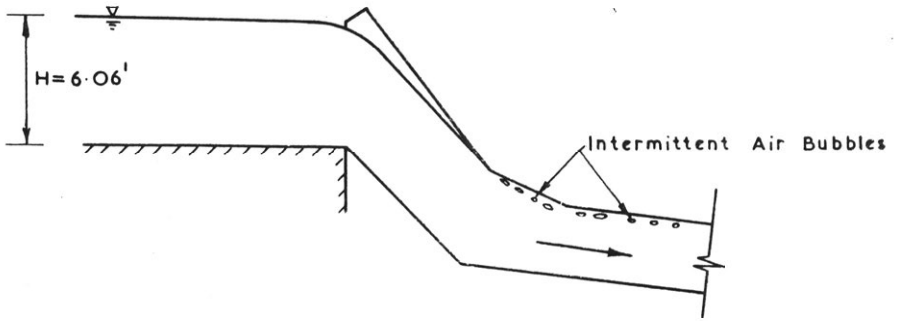

(b) Q=310 c.f.s. CRITICAL DISCHARGE FOR FREE SURFACE FLOW AND PIPE-FULL FLOW

FIGURE 25: FLOW PROFILES NEAR INLET TRANSITION: UNVENTED CONDITIONS CE-E-6761

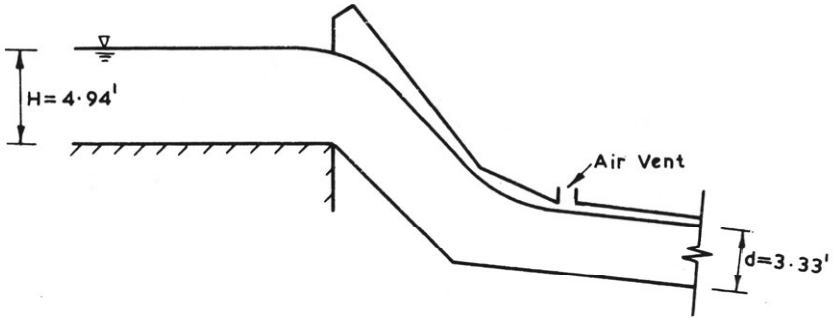

(a) Q=204 c.f.s. FREE SURFACE FLOW

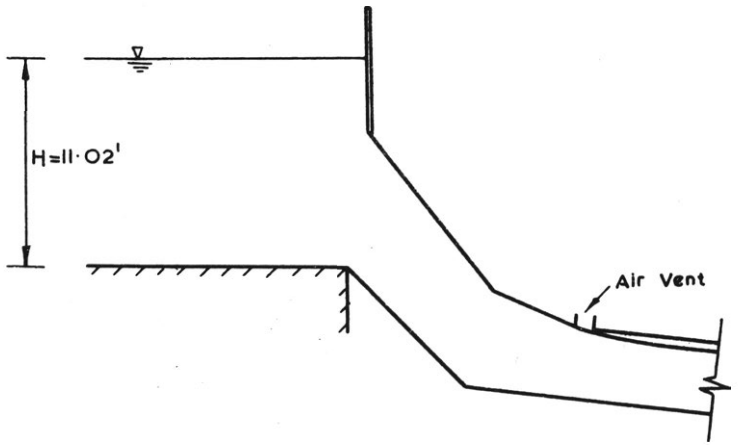

(c) Q=300 c.f.s. SLUICE FLOW WITH OCCASIONAL PIPE-FULL FLOW DOWNSTREAM

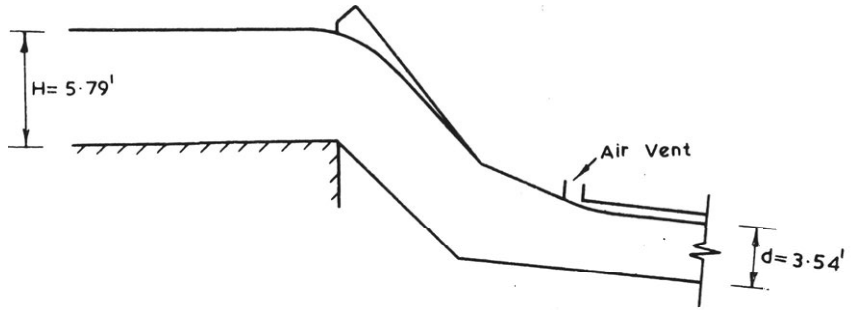

(b) Q=242 c.f.s. CRITICAL DISCHARGE FOR FREE SURFACE FLOW AND SLUICE FLOW

FIGURE 26: FLOW PROFILES NEAR INLET TRANSITION: VENTED CONDITIONS CE-E-6762

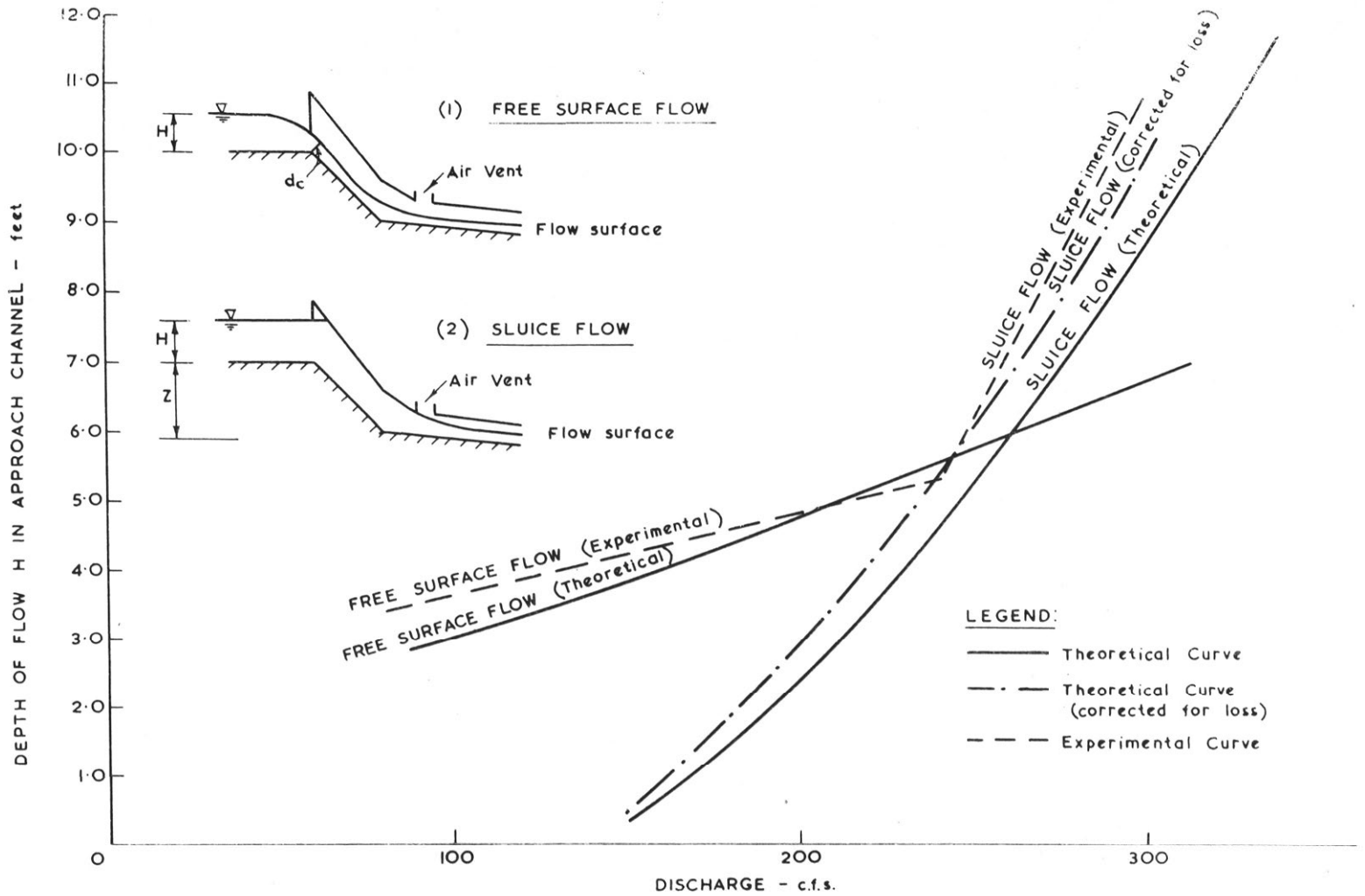

FIGURE 27: REGIME OF FLOW IN PIPE INLET TRANSITION WITH UPSTREAM AIR VENT CE-E-6763

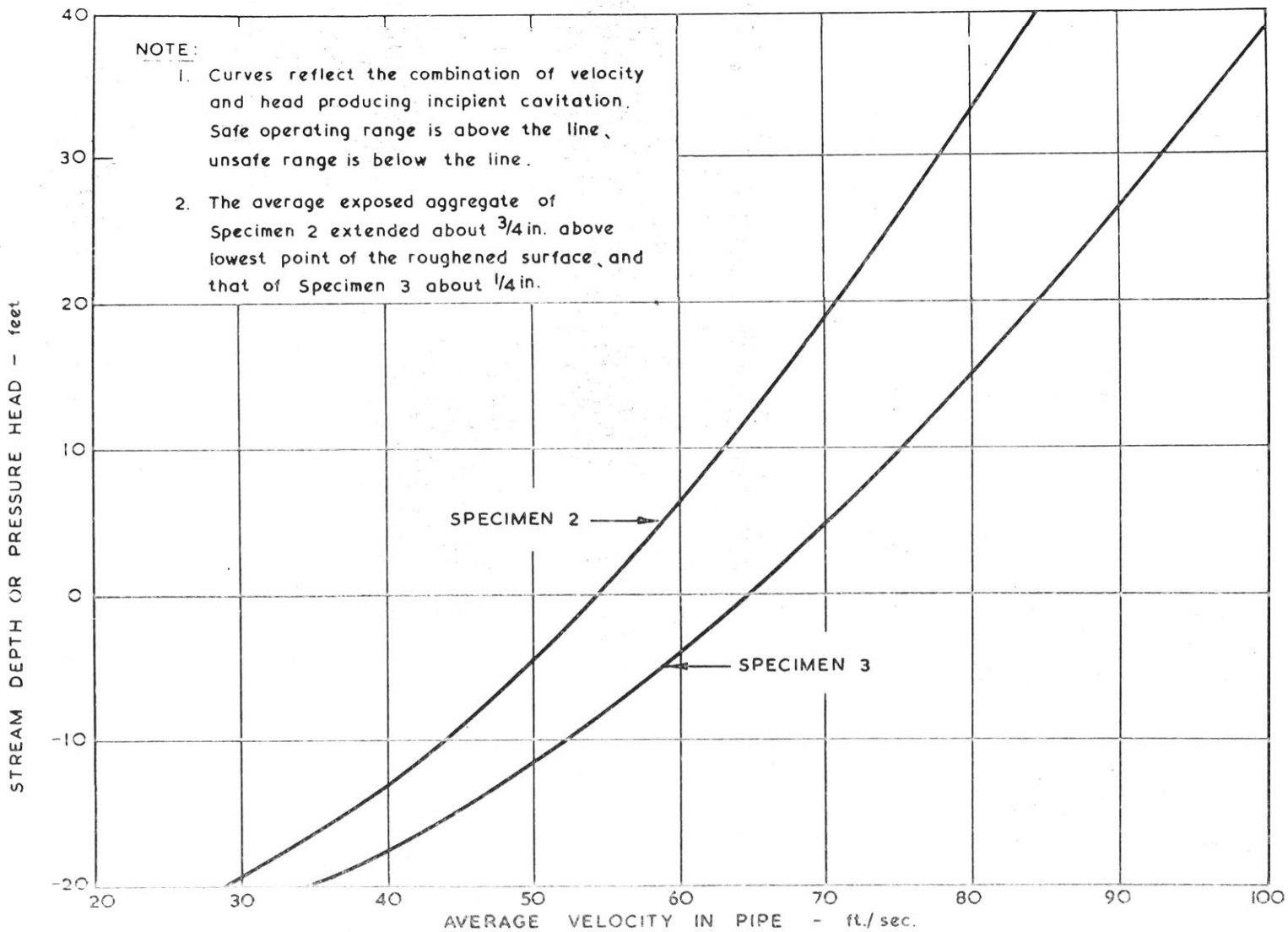

FIGURE 28: RELATIONSHIP BETWEEN STREAM DEPTH (OR PRESSURE HEAD) AND AVERAGE STREAM VELOCITY. (After D. Colgate) CE-E-6768

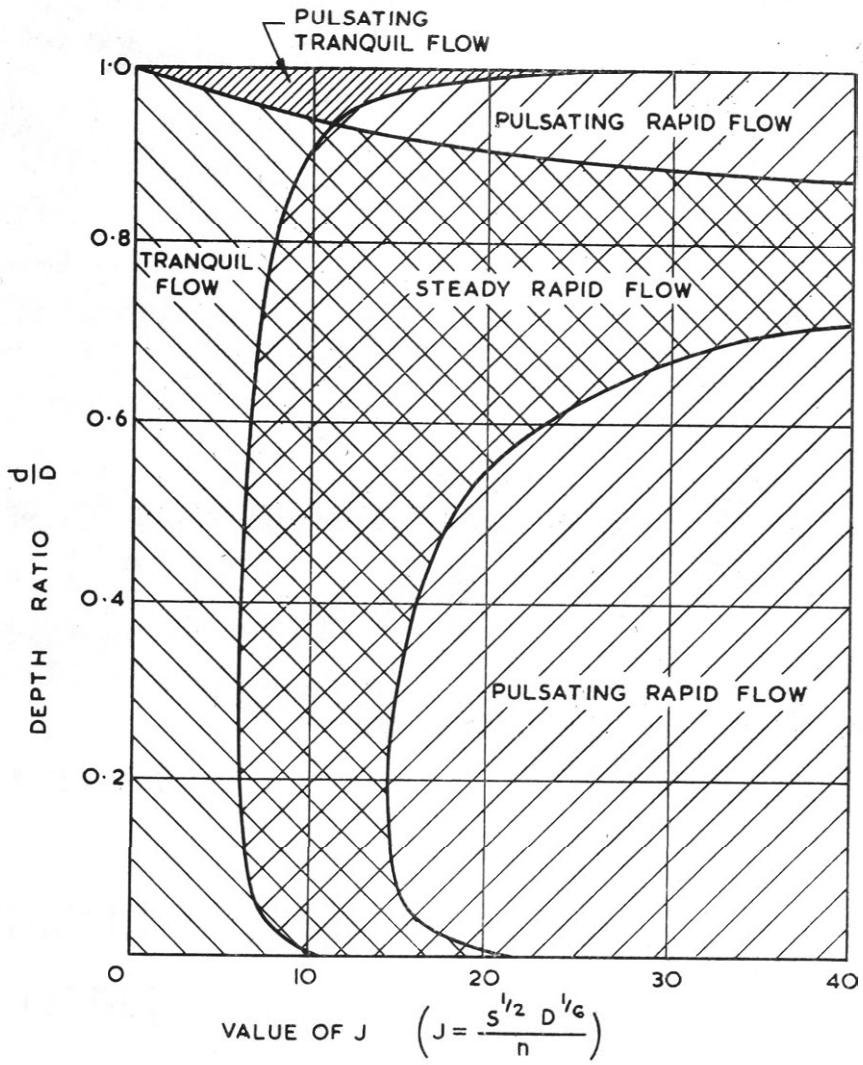

FIGURE 29: VARIOUS TYPES OF FLOWS IN PIPE

(After F. F. Escoffier and M. B. Boyd)

CE - E - 6769